# The deubiquitinase Ubp3/Usp10 constrains glucose-mediated mitochondrial repression via phosphate budgeting

Vineeth Vengayil[1,2], Shreyas Niphadkar[1,2], Swagata Adhikary[1,2], Sriram Varahan[1], Sunil Laxman[1]*

1. Institute for Stem Cell Science and Regenerative Medicine (DBT-inStem)
   GKVK Post Bellary Road
   Bangalore 560065
2. Manipal Academy of Higher Education, Manipal, Karnataka 576104, India

*correspondence: sunil@instem.res.in

**Keywords:** mitochondria, glycolysis, phosphate, deubiquitinase, Crabtree

## Abstract

Many cells in high glucose repress mitochondrial respiration, as observed in the Crabtree and Warburg effects. Our understanding of biochemical constraints for mitochondrial activation is limited. Using a *Saccharomyces cerevisiae* screen, we identified the conserved deubiquitinase Ubp3 (Usp10), as necessary for mitochondrial repression. Ubp3 mutants have increased mitochondrial activity despite abundant glucose, along with decreased glycolytic enzymes, and a rewired glucose metabolic network with increased trehalose production. Utilizing *Δubp3* cells, along with orthogonal approaches, we establish that the high glycolytic flux in glucose continuously consumes free Pi. This restricts mitochondrial access to inorganic phosphate (Pi), and prevents mitochondrial activation. Contrastingly, rewired glucose metabolism with enhanced trehalose production and reduced GAPDH (as in *Δubp3* cells) restores Pi. This collectively results in increased mitochondrial Pi and derepression, while restricting mitochondrial Pi transport prevents activation. We therefore suggest that glycolytic-flux dependent intracellular Pi budgeting is a key constraint for mitochondrial repression.

## Introduction

Rapidly proliferating cells have substantial metabolic and energy demands in order to increase biomass (Cai and Tu, 2012; Zhu and Thompson, 2019). This includes a high ATP demand, obtained from cytosolic glycolysis or mitochondrial oxidative phosphorylation (OXPHOS), to fuel multiple reactions (Nelson et al., 2008). Interestingly, many rapidly proliferating cells preferentially rely on ATP from glycolysis/fermentation over mitochondrial respiration even in oxygen-replete conditions, and is the well-known Warburg effect (Vander Heiden et al., 2009; Warburg, 1925). Many such cells repress mitochondrial processes in high glucose, termed glucose-mediated mitochondrial repression or the Crabtree effect (Crabtree, 1929; De Deken, 1966). This is observed in some tumors (Vander Heiden et al., 2009), neutrophils (Xia et al., 2021), activated macrophages (Kornberg, 2020), stem cells (Abdel-Haleem et al., 2017; Pacini and Borziani, 2014; Tsogtbaatar et al., 2020), and famously *Saccharomyces cerevisiae* (De Deken, 1966). Numerous studies have identified signaling programs or regulators of glucose-mediated mitochondrial repression. However, biochemical programs and regulatory processes in biology evolve around key biochemical constraints (Cornish-Bowden, 2016). The biochemical constraints for mitochondrial repression remain unresolved (Diaz-Ruiz et al., 2011; Hammad et al., 2016).

There are two hypotheses on the biochemical principles driving mitochondrial repression. The first proposes direct roles for glycolytic intermediates in driving mitochondrial respiration, by inhibiting specific mitochondrial outputs (Díaz-Ruiz et al., 2008; Lemus et al., 2018). The second hypothesizes that a competition between glycolytic and mitochondrial processes for mutually required metabolites/co-factors such as pyruvate, ADP or inorganic phosphate (Pi) could determine the extent of mitochondrial repression (Diaz-Ruiz et al., 2011; Hammad et al., 2016; Koobs, 1972). These are not all mutually exclusive, and a combination of these factors might dictate mitochondrial repression in high glucose. However, any hierarchies of importance are unclear (Rodríguez-Enríquez et al., 2001), and experimental data for the necessary constraints for mitochondrial repression remains incomplete.

One approach to resolve this question has been to identify regulators of metabolic state under high glucose. Post-translational modifications (PTMs) regulated by signaling systems can regulate mitochondrial repression (Broach, 2012; Hitosugi and Chen, 2014; Tripodi et al., 2015). Ubiquitination is a PTM that regulates global proteostasis (Hershko and Ciechanover, 1998; Komander and Rape, 2012), but the roles of ubiquitination-dependent

processes in regulating mitochondrial repression are poorly explored. Ubiquitination itself is determined by the balance between ubiquitination, and deubiquitinase (DUB) dependent deubiquitination (Pickart and Eddins, 2004). Little is known about the roles of DUBs in regulating metabolic states, making the DUBs interesting candidate regulators of mitochondrial repression.

In this study, using an *S. cerevisiae* DUB knock-out library-based screen, we identified the evolutionarily conserved deubiquitinase Ubp3 (mammalian Usp10) as required for mitochondrial repression in high glucose. Loss of Ubp3 resulted in mitochondrial activation, along with a reduction in the glycolytic enzymes-phosphofructokinase 1 (Pfk1) and GAPDH (Tdh2 and Tdh3). This consequently reroutes glucose flux and increases trehalose biosynthesis. This metabolic rewiring increases Pi release from trehalose synthesis, and decreases Pi consumption in glycolysis, to cumulatively increase Pi pools. Using *ubp3Δ* cells along with independent analysis of wild-type cells, and isolated mitochondrial fractions, we establish that glycolytic-flux dependent Pi allocations to mitochondria determines mitochondrial activity. Through these data, we propose how intracellular Pi balance as controlled by glycolytic flux, is a biochemical constraint for mitochondrial repression.

## Results

### A deubiquitinase deletion screen identifies Ubp3 as a regulator of glucose-mediated mitochondrial repression

In cells such as *S. cerevisiae*, high glucose represses mitochondrial activity as well as OXPHOS-dependent ATP synthesis (De Deken, 1966; Postma et al., 1989) (illustrated in Figure 1A). Our initial objective was to identify proteostasis regulators of glucose-mediated mitochondrial repression. We generated and used a deubiquitinase (DUB) deletion strain library of *S. cerevisiae* (Figure 1-figure supplement 1A), to unbiasedly identify regulators of mitochondrial repression by measuring the fluorescence intensity of a potentiometric dye Mitotracker CMXRos (illustrated in Figure 1B). Using this screen, we identified DUB mutants with altered mitochondrial membrane potential (Figure 1C, Figure 1-figure supplement 1 A). Note: WT cells in a respiratory medium (2% ethanol) were used as a control to estimate maximum mitotracker fluorescence intensity (Figure 1-figure supplement 1B).

93 A prominent 'hit' was the evolutionarily conserved deubiquitinase Ubp3 (Figure 1C),
94 (homologous to mammalian Usp10) (Figure 1-figure supplement 1D). Due to its high degree
95 of conservation across eukaryotes (Figure 1-figure supplement 1D) as well as putative roles in
96 metabolism or mitochondrial function (Isasa et al., 2015; Nostramo et al., 2016; Ossareh-
97 Nazari et al., 2010), we focused our further attention on this DUB. Cells lacking Ubp3 showed
98 an ~1.5-fold increase in mitotracker fluorescence (Figure 1C, Figure 1-figure supplement 1A,
99 C). Cells with catalyticaly inactive Ubp3 ($Ubp3^{C469A}$), showed increased mitochondrial
100 potential comparable to *ubp3Δ* (Figure 1D). This data confirmed that Ubp3 catalytic activity
101 of is required to fully repress mitochondrial activity under high glucose. The catalytic site
102 mutation did not affect steady-state Ubp3 levels (Figure 1-figure supplement 1E).

103 Next, to assess the requirement of Ubp3 for mitochondrial function, we quantified the
104 electron transport chain (ETC) complex IV subunit Cox2 (Fontanesi et al., 2006)(Figure 1E).
105 *ubp3Δ* had higher Cox2 than WT (Figure 1E). As a control, we estimated total mitochondrial
106 content in WT and *ubp3Δ* cells, using either estimates of the structural protein Tom70, or
107 measuring the fluorescence-intensity in strains engineered with mitochondrial targeted
108 mNeonGreen (Dua et al., 2022). There was no increase in the total mitochondrial volume
109 (estimated by measuring the intensity of mitochondria targeted mNeon green) (Figure 1-
110 figure supplement 1F) or mitochondrial outer membrane protein Tom70 (Figure 1-figure
111 supplement 1G). This suggests that the increased Cox2 is not merely because of higher total
112 mitochondrial content. We next measured the basal oxygen consumption rate (OCR) of
113 *ubp3Δ*, and basal OCR was higher in *ubp3Δ*, indicating higher respiration (Figure 1F).

114 Next, we asked if mitochondrial ATP synthesis was higher in *ubp3Δ*. The total ATP
115 levels in WT and *ubp3Δ* were comparable (Figure 1G). However, upon treatment with the ETC
116 complex IV inhibitor sodium azide, ATP levels in WT were higher than *ubp3Δ*, contributing to
117 ~60% of the total ATP (Figure 1H). In contrast, the ATP levels in *ubp3Δ* after sodium azide
118 treatment were ~ 40% of the total ATP (Figure 1H). These data suggest a higher contribution
119 of mitochondrial ATP synthesis towards the total ATP pool in *ubp3Δ*.

120 We next asked if *ubp3Δ* required higher mitochondrial activity for growth, using a
121 series of mitochondrial activity inhibitors and comparing relative growth. In high glucose, WT
122 cells show minimal growth inhibition in the presence of sodium azide, indicating lower

123 reliance on mitochondrial function (Figure 1I). Contrastingly, *ubp3Δ* or Ubp3$^{C469A}$ show a
124 severe growth defect in the presence of the mitochondrial ETC complex inhbitors sodium
125 azide and oligomycin, and the mitochondrial OXPHOS uncoupler FCCP (Figure 1I, Figure 1-
126 figure supplement 1H). Additionally, the loss of Ubp3 in respiration defective cox2-62 cells
127 (Bonnefoy et al., 2001), or Rho0 cells (which lacks mitochondrial DNA) resulted in a severe
128 growth defect (Figure 1-figure supplement 1I). Deletion of ATP synthase subunits Atp1 and
129 Atp10 also results in a severe growth defect in *ubp3Δ* compared to WT (Figure 1-figure
130 supplement 1I). Together, these results indicate that the loss of Ubp3 makes cells dependent
131 on mitochondrial ATP synthesis in high glucose.

132 In order to address whether the deletion of Ubp3 might increase ubiquitinated
133 proteins and consequent proteostatic stress, we analysed the global ubquitination state in
134 *ubp3Δ* cells. WT and *ubp3Δ* cells grown under brief (1 hour) heat stress, which increases
135 protein ubiquitination, was used as a control. However, we did not observe a significant
136 increase in the global ubiqutinatin state in *ubp3Δ* cells (Figure 1-figure supplement 1J). This
137 suggests that the altered mitochondrial metabolism in *ubp3Δ* cells is unlikely to be due to
138 proteostatic stress.

139 Collectively these data show that in 2% glucose, *ubp3Δ* have high mitochondrial
140 activity, respiration, and rely on this mitochondrial function for ATP production and growth.
141 We therefore decided to use *ubp3Δ* cells to start delineating requirements for glucose-
142 mediated mitochondrial repression.

143

144 **Key glycolytic enzymes decrease and glucose flux is rerouted in *ubp3Δ* cells**

145 Glucose-6 phosphate (G6P) is the central node in glucose metabolism where carbon-
146 allocations are made towards distinct metabolic arms, primarily: glycolysis, the pentose
147 phosphate pathway (PPP), and trehalose biosynthesis (Figure 2A). We first compared
148 amounts of two key ('rate-controling') glycolytic enzymes - Phosphofructokinase 1 (Pfk1),
149 GAPDH isozymes (Tdh2, Tdh3) (Nelson et al., 2008), along with the enolase isozymes (Eno1,
150 Eno2) in WT and *ubp3Δ* cells. Pfk1, Tdh2, and Tdh3 substantially decreased in *ubp3Δ* (but not
151 Eno1 and Eno2) (Figure 2B, Figure 2-figure supplement 1A). Since deubiquitinases can control

152 protein amounts by regulating proteasomal degradation, we asked if the decrease in Pfk1,
153 Tdh2 and Tdh3 in *ubp3Δ* is due to proteasomal degradation. To test this, we measured the
154 levels of these enzymes in *ubp3Δ* after treatement with proteasomal inhibitor MG132. We
155 did not observe any rescue in the levels of these enzymes in MG132 treated samples,
156 suggesting that the decreased levels of these enzymes were not due to increased proteasomal
157 degradation (Figure 2-figure supplement 1B). To further understand if these enzyme
158 transcripts are altered in *ubp3Δ*, we measured the mRNA levels of PFK1, TDH2 and TDH3 in
159 WT, *ubp3Δ* and Ubp3$^{C469A}$ cells. The transcripts of all the three genes in *ubp3Δ* and Ubp3$^{C469A}$
160 cells decreased (Figure 2-figure supplement 1C), suggesting that Ubp3 regulates the
161 transcripts of these glycolytic enzyme genes. The reduction in the Pfk and GAPDH enzyme
162 amounts was intriguing, because the Pfk and GAPDH steps are critical in determining
163 glycolytic flux (Nelson et al., 2008; Shestov et al., 2014). A reduction in these enzymes could
164 therefore decrease glycolytic flux, and would reroute glucose (G6P) allocations via mass
165 action towards other branches of glucose metabolism, primarily the pentose phosphate
166 pathway as well as trehalose biosynthesis (Figure 2A). To assess this, we first measured the
167 steady-state levels of key glycolytic and pentose phosphate pathway (PPP) intermediates, and
168 trehalose in WT or *ubp3Δ* using targeted LC-MS/MS (Figure 2C, Figure 2-figure supplement
169 1D). Glucose-6/fructose-6 phosphate (G6P/F6P) increased in *ubp3Δ* (Figure 2C). Concurrently,
170 trehalose, and the PPP intermediates ribose 5-phosphate (R5P) and sedoheptulose 7-
171 phosphate (S7P), increased in *ubp3Δ* (Figure 2C).

172 Since steady-state metabolite amounts cannot separate production from utilization,
173 in order to unambiguously assess if glycolytic flux is reduced in *ubp3Δ* cells, we utilized a pulse
174 labeling of $^{13}C_6$ glucose, following which the label incorporation into glycolytic and other
175 intermediates was measured. Note that because glycolytic flux is very high in yeast, this
176 experiment would require rapid pulsing and extraction of metabolites in order to stay in a
177 linear range and avoid label saturation. We therefore established a very short time point of
178 label-addition, quenching and metabolite extraction post $^{13}C$ glucose pulse. Since flux
179 saturates/reaches steady-state in seconds, we first ensured that the label incorporation into
180 individual metabolites after the $^{13}C$ glucose pulse was in the linear range, and for early
181 glycolytic intermediates this was seconds after glucose addition. This new methodology is
182 extensively described in materials and methods, with required controls shown in Figure 2-

183 figure supplement 1F. WT and *ubp3Δ* cells were grown in high glucose, pulsed with $^{13}C_6$
184 glucose, and the relative $^{13}C$ label incorporation into glycolytic intermediates and trehalose
185 were measured, as shown in the schematic (Figure 2-figure supplement 1E). In *ubp3Δ,* $^{13}C$
186 label incorporation into G6P/F6P as well as trehalose substantially increased (Figure 2D).
187 Contrastingly, $^{13}C$ label incorporation into glycolytic intermediates F1,6BP, G3P, 3PG and PEP
188 decreased, indicating decreased glycolytic flux (Figure 2D). We next measured ethanol
189 concentrations and production rates, as an additional output of relative glycolytic rates. We
190 observed decreased steady-state ethanol levels, as well as ethanol production rates in *ubp3Δ*
191 (Figure 2F).

192 Glycolysis-derived pyruvate is transported to mitochondria and fuels the TCA cycle.
193 Therefore, we asked if the decreased glycolytic rate result in a decrease in the TCA cycle flux
194 as well. To test this, we first measured the steady state levels of TCA cycle intermediates in
195 WT or *ubp3Δ* using targeted LC-MS/MS. We did not observe any significant change in the
196 levels of TCA cycle intermediates in *ubp3Δ,* except malate which showed a significant
197 decrease in *ubp3Δ* (Figure 2-figure supplement 2A). Next, in order to assess if TCA cycle flux
198 reduces in *ubp3Δ* cells, WT and *ubp3Δ* cells were grown in high glucose, pulsed with $^{13}C_6$
199 glucose, and the relative $^{13}C$ label incorporation into TCA cycle intermediates was measured,
200 as shown in the schematic (Figure 2-figure supplement 2B). The kinetics of $^{13}C$ label
201 incorporation in TCA cycle intermediates are shown in Figure 2-figure supplement 2C. We did
202 not observe any significant change in the relative $^{13}C$ label incorporation in TCA cycle
203 intermediates in *ubp3Δ.* Therefore, these data suggest that the decreased glycolytic flux in
204 *ubp3Δ* does not result in a decrease in TCA cycle flux. The increased respiration and
205 mitochondrial activity in *ubp3Δ* cells is therefore driven via other factors.

206 Collectively, these results reveal that that reduced Pfk1 and GAPDH (in *ubp3Δ*)
207 decrease glucose flux via glycolysis, which results in rewired glucose flux towards trehalose
208 biosynthesis and the PPP.

209

210 **Rerouted glucose flux results in phosphate (Pi) accumulation**

211 We therefore asked if the proteomic state, as observed in *ubp3Δ* cells, could provide
212 clues to explain the coupling between mitochondrial derepression and rerouted glucose flux.
213 A recent study by Isasa et al., had systematically quantified the changes in protein levels in
214 *ubp3Δ* cells (Isasa et al., 2015). We therefore reanalyzed this extensive dataset, looking for
215 changes in proteins that would correlate with these metabolic processes. Notably, we
216 observed increased levels of proteins of the mitochondrial ETC and respiration, and decreased
217 amounts of glucose metabolizing enzymes in *ubp3Δ* (Figure 3A). Additionally, multiple
218 proteins involved in regulating phosphate (Pi) homeostasis were decreased in *ubp3Δ* (Figure
219 3A) (Isasa et al., 2015). We had recently uncovered a reciprocal coupling of Pi homeostasis
220 with the different arms of glucose metabolism, particularly trehalose biosynthesis (Gupta et
221 al., 2019; Gupta and Laxman, 2021), and therefore wondered if a glycolytic-flux dependent
222 change in Pi homeostatsis had any role in mitochondrial respiration. Our hypothesis was
223 refined based on the reasoning given below.

224 One explanation for mitochondrial repression can be an internal competition for
225 shared metabolites/co-factors between (cytosolic) glycolytic and mitochondrial processes,
226 that mitochondria might not be sufficiently able to access (Diaz-Ruiz et al., 2011; Koobs, 1972;
227 Rodríguez-Enríquez et al., 2001). In this context, a plausible role for inorganic phosphate (Pi)
228 in regulating mitochondrial repression can be hypothesized. Cytosolic glycolysis requires
229 rapid, high consumption of net Pi (Mason et al., 1981; Rodríguez-Enríquez et al., 2001; Van
230 Heerden et al., 2014), and this could possibly limit the Pi that is continuously available for
231 mitochondrial use (Brazy et al., 1982; Koobs, 1972), thereby repressing mitochondria.
232 Contextually, the balance between reactions releasing vs consuming Pi could explain changes
233 in global Pi levels (Gupta and Laxman, 2021). A continuous hub of Pi consumption is glycolysis.
234 Here, GAPDH catalyzes G3P to 1,3BPG, converting ADP to ATP, while concurrently consuming
235 a molecule of Pi (Hohmann et al., 1996; Van Heerden et al., 2014). This Pi that goes into ATP
236 will subsequently be used for nucleotide biosynthesis, polyphosphate biosynthesis and
237 protein phosphorylation (Gupta and Laxman, 2021; Hunter, 2012). Therefore, we can surmise
238 that in high glycolytic flux, the production of ATP, nucleotides and polyphosphates is
239 concurrent with Pi consumption (Austin and Mayer, 2020; Hohmann et al., 1996; Ljungdahl
240 and Daignan-Fornier, 2012). Could this reaction therefore limit cytosolic Pi for the
241 mitochondria (as illustrated in Figure 3B)? Notably, *ubp3Δ* have reduced GAPDH levels and

242 decreased glycolytic flux. Second, trehalose synthesis is a Pi releasing reaction, and a major
243 source of free Pi that is critical for Pi homeostasis (Gupta et al., 2019; Van Heerden et al.,
244 2014). Flux through this reaction is also substantially higher in *ubp3Δ*. Therefore, these cells
245 might have increased Pi release (via trehalose), coupled with decreased Pi consumption (via
246 decreased GAPDH). We therefore asked if total Pi increases in *ubp3Δ* (Figure 3B)?

247 To test this, we directly assessed total Pi levels in *ubp3Δ* and WT. *ubp3Δ* cells had
248 higher Pi than WT, and this was comparable to Pi in WT grown in excess Pi (Figure 3C).
249 Similarly, Pi amounts also increased in Ubp3$^{C469A}$ (Figure 3-figure supplement 1A). Therefore,
250 the loss of Ubp3 increases intracellular Pi levels. Next, we asked if *ubp3Δ* cells exhibit
251 signatures of a 'high Pi' state. *S. cerevisiae* maintains internal Pi balance by controlling the
252 expression of multiple genes collectively known as the Pho regulon (Mouillon and Persson,
253 2006). The Pho regulon is induced under Pi limitation, and repressed during Pi sufficiency
254 (Gupta et al., 2019; Mouillon and Persson, 2006). We assessed two major Pho proteins
255 (Pho84: a high-affinity membrane Pi transporter, and Pho12: an acid phosphatase) in WT and
256 *ubp3Δ* in high glucose. *ubp3Δ* cells have lower amounts of Pho84 and Pho12 (Figure 3D).
257 Further, upon shifting to low Pi for one hour, Pho84 and Pho12 increased in *ubp3Δ*. These
258 data suggest that reduced Pho84 and Pho12 amounts in *ubp3Δ* are because of increased Pi,
259 and not due to altered Pho regulon function itself (Figure 3D). These data clarify earlier
260 observations from *ubp3Δ* which noted reduced Pho proteins (Isasa et al., 2015). Therefore,
261 *ubp3Δ* constitutively have higher Pi, and likely a consequent decrease in Pho proteins.

262 We next asked if the increased Pi in *ubp3Δ* is because of altered G6P allocations
263 towards different end-points, particularly trehalose synthesis, which can be a major node of
264 Pi restoration (Gupta et al., 2019; Van Heerden et al., 2014). We assessed the contribution of
265 increased trehalose synthesis towards the high Pi in *ubp3Δ*, by estimating Pi levels in the
266 absence of trehalose 6-phosphate phosphatase (Tps2), which catalyzes the Pi-releasing step
267 in trehalose synthesis. Notably, loss of Tps2 in *ubp3Δ* decreased Pi (Figure 3E). There was no
268 additive difference in Pi between *tps2Δ* and *ubp3Δtps2Δ* (Figure 3E). As an added control, we
269 assessed trehalose in WT and *ubp3Δ* in the absence of Tps2, and found no difference (Figure
270 3-figure supplement 1B). Therefore, increasing G6P flux towards trehalose biosynthesis is a
271 major source of the increased Pi in *ubp3Δ*.

272 Since the major GAPDH isozymes, Tdh2 and Tdh3, are reduced in *ubp3Δ*, we directly
273 asked if reducing GAPDH can decrease Pi consumption and increase Pi. To assess this, we
274 generated *tdh2Δtdh3Δ* cells, which exhibit a growth defect, but are viable, permitting further
275 analysis. *tdh2Δtdh3Δ* had higher Pi in high glucose (Figure 3F). Expectedly, we observed a
276 decrease in ethanol in *tdh2Δtdh3Δ* (Figure 3-figure supplement 1C), along with an
277 accumulation of F1,6 BP and G3P, and decreased 3PG and PEP (Figure 3-figure supplement
278 1D). However, G6P and trehalose levels between WT and *tdh2Δtdh3Δ* were comparable
279 (Figure 3-figure supplement 1D, E). These data sugest that unlike in *ubp3Δ*, the increased Pi
280 in *tdh2Δtdh3Δ* comes mainly from decreased Pi consumption (GAPDH step). To further assess
281 the role of reduced glycolytic flux in increasing Pi (*ubp3Δ* and *tdh2Δtdh3Δ*), we measured the
282 Pi in these cells growing in a gluconeogenic medium – 2%, ethanol. In this scenario, the GAPDH
283 catalyzed reaction will be reversed, converting 1,3BPG to G3P, which should release and not
284 consume Pi. Compared to WT, the Pi levels decreased in *ubp3Δ* and *tdh2Δtdh3Δ* (Figure 3G),
285 suggesting that the changes in Pi in these mutants is driven by the relative change in Pi release
286 vs consumption.

287 These results collectively indicate that the combined effect of increased Pi release
288 coming from trehalose synthesis, and decreased Pi consumption from reduced GAPDH
289 increase Pi levels in *ubp3Δ*.

290

291 **Mitochondrial Pi availability correlates with mitochondrial activity in *ubp3Δ***

292 We therefore wondered if this observed Pi increase from the combined rewiring of
293 glucose metabolism resulted in more Pi becoming accessible to the mitochondria. This would
294 effectively result in Pi budgeting between cytosolic glycolysis and mitochondria based on the
295 relative flux in different arms of glucose metabolism, by increasing Pi availability for the
296 mitochondria (Figure 4A). If this were indeed so, a prediction would be that the pool of Pi in
297 the mitochondria of *ubp3Δ* cells would be higher than WT cells, while the opposite would be
298 expected in the cytosolic fraction of these cells, due to increased Pi in the mitochondria. To
299 test if this were so, we first measured the cytosolic pools of Pi in WT and *ubp3Δ.* The cytosolic
300 fraction was isolated (extensive experimental details are in the SI appendix) from WT and

301 *ubp3Δ* cells, and Pi levels in this fraction were estimated (Figure 4B, Figure 4-figure
302 supplement 1B). We observed significantly reduced Pi in the cytosolic fraction in *ubp3Δ* cells.
303 Since total cellular Pi amounts is higher in *ubp3Δ* cells (Figure 3), a decreased cytolosolic Pi
304 would be consistent with greater transport of Pi from cytosol to other organelles such as
305 vacuole (where it is stored as polyphosphate) and/or mitochondria. Therefore, we next asked
306 if the mitochondria in *ubp3Δ* have correspondingly increased Pi. Mitochondria were isolated
307 by immunoprecipitation from WT and *ubp3Δ*, the isolation efficiency was analyzed (Figure 4-
308 figure supplement 1A), and relative Pi levels compared. Pi levels were normalised to Idh1
309 (isocitrate dehydrogenase) in isolated mitochondria, since Idh1 protein levels did not
310 decrease in *ubp3Δ* (Figure 4-figure supplement 1B), and consistent with (Isasa et al., 2015).
311 Mitochondrial Pi was higher in *ubp3Δ* (Figure 4B). We next asked if the increased
312 mitochondrial activity in *ubp3Δ* is a consequence of high Pi. If this were so, *tdh2Δtdh3Δ* should
313 partially phenocopy *ubp3Δ* with respect to mitochondrial activity. Consistently, *tdh2Δtdh3Δ*
314 have higher mitotracker intensity as well as Cox2 levels compared to WT (Figure 4-figure
315 supplement 1C, Figure 4C). Also consistent with this, a high basal OCR in *tdh2Δtdh3Δ* was
316 observed (Figure 4D), together indicating high mitochondrial activity in *tdh2Δtdh3Δ*, which is
317 comparable to *ubp3Δ*.

318 We next asked if higher Pi is necessary to increase mitochondrial activity in *ubp3Δ* and
319 *tdh2Δtdh3Δ*. Since glycolysis is defective in *ubp3Δ* and *tdh2Δtdh3Δ*, it is necessary to
320 distinguish the effect of high Pi vs. only the effect of low glycolysis in activating mitochondria.
321 Logically, if decreased glycolysis (independent of Pi) is sufficient to activate mitochondria,
322 bringing down the Pi levels in *ubp3Δ* to that of WT should not affect mitochondrial activity.
323 Notably, *ubp3Δ* grown in low (1 mM) Pi have Pi levels similar to WT in standard (normal Pi)
324 medium (Figure 4-figure supplement 1D). *ubp3Δ* grown in low Pi also had decreased ethanol,
325 suggesting reduced glycolysis (Figure 4-figure supplement 1E). Therefore, we used this
326 condition to further understand the role of Pi in inducing mitochondrial activity. Mitotracker
327 fluorescence decreased in both *ubp3Δ* and *tdh2Δtdh3Δ* in low Pi (Figure 4-figure supplement
328 1F). Note: basal mitotracker fluorescence in WT also decreases in low Pi, which is consistent
329 with a required role of Pi for mitochondrial activity (Figure 4-figure supplement 1F). Similarly,
330 Cox2 levels were reduced in both *ubp3Δ* and *tdh2Δtdh3Δ* (Figure 4E). Consistent with both
331 reduced mitotracker intensity and Cox2 levels, basal OCR also decreased in both *ubp3Δ* and

332 *tdh2Δtdh3Δ* in low Pi (Figure 4F). As an additional control, we used Rho0 strains (which have
333 no mitochondrial DNA and therefore lack functional ETC) to compare basal OCR. The
334 expectation in these strains is that basal OCR will not change if Pi changes. Consistently, we
335 did not observe any significant difference in basal OCR in WT, *ubp3Δ* and *ubp3Δ* in low Pi in a
336 Rho0 strain background (which lacks mitochondrial DNA) (Figure 4-figure supplement 1G).
337 These data collectively suggest that high intracellular Pi is necessary to increase mitochondrial
338 activity in *ubp3Δ* and *tdh2Δtdh3Δ*.

339 Next, we asked how mitochondrial Pi transport regulates mitochondrial activity. Mir1
340 and Pic2 are mitochondrial Pi transporters, with Mir1 being the major Pi transporter
341 (Murakami et al., 1990; Zara et al., 1996). We first limited mitochondrial Pi availability in
342 *ubp3Δ* by knocking-out *MIR1*. In *mir1Δ*, the increased Cox2 observed in *ubp3Δ* was no longer
343 observed (Figure 4G). Consistent with this, we observed no further increase in the basal OCR
344 in *mir1Δubp3Δ* compared to *mir1Δ* (Figure 4H). Furthermore, *mir1Δ* showed decreased Cox2
345 as well as basal OCR even in WT cells (Figure 4G, Figure 4H). These data together suggest that
346 mitochondrial Pi transport is critical for increasing mitochondrial activity in *ubp3Δ*, and in
347 maintaining basal mitochondrial activity even in high glucose.

348 As a control, no significant increase in Mir1 and Pic2 was observed in *ubp3Δ* (Figure 4-
349 figure supplement 1H), suggesting that *ubp3Δ* do not increase mitochondrial Pi by merely
350 increasing the Pi transporters, but rather by increasing available Pi pools.

351 Taken together, these data suggest the possibility that the altered Pi homeostais in
352 *ubp3Δ* cells increases the mitochondrial Pi pool. This increased mitochondrial Pi pool
353 correlates with increased mitochondrial activity. Decreasing mitochondrial Pi by either
354 reducing total Pi, or by reducing mitochondrial Pi transport decreases mitochondrial activity.

355

356 **Mitochondrial Pi availability constrains mitochondrial activity under high glucose**

357 So far, these data suggest that the cytosolic Pi available for the mitochondria can
358 determine the extent of mitochondrial activity. Therefore, we further investigated if

359 mitochondrial Pi allocation was a necessary constraint for glucose-mediated mitochondrial
360 repression.

361 To test this, we first asked how important mitochondrial Pi transport was to switch to
362 increased respiration. In WT yeast, low glucose or glycolytic inhibition will result in increased
363 respiration (Broach, 2012). What happens therefore if we restrict mitochondrial Pi in this
364 context? For this, we measured the basal OCR in WT and *mir1Δ* after switching from high (2%)
365 to low (0.1%) glucose. We observed a significant increase in the basal OCR in WT but not in
366 *mir1Δ* (Figure 5A). The alternate scenario is after glycolytic inhibition. We assessed the role of
367 mitochondrial Pi in this context, by inhibiting glycolysis using 2-deoxyglucose (2DG). WT, but
368 not *mir1Δ*, increased their OCR (respiration) upon a 1-hour treatment with 2DG (Figure 5B).
369 Consistent with this, mitotracker fluorescence increased with an increase in 2DG in WT, but
370 not in *mir1Δ* (Figure 5-figure supplement 1A). We further asked if the mitochondrial Pi
371 transporter itself glucose repressed, and therefore assessed Mir1 amounts in high and low
372 glucose. Mir1 levels are higher upon a shift to low glucose, and in cells grown in 2% ethanol,
373 suggesting that Mir1 is glucose repressed (Figure 5C, Figure 5-figure supplement 1B). These
374 data suggest that mitochondrial Pi transport is necessary for increasing mitochondrial activity
375 after glucose derepression.

376 We next asked whether just adding external Pi was sufficient to increase
377 mitochondrial activity, when cells are in high glucose. In medium supplemented with excess
378 Pi, the internal Pi increases as seen earlier (Figure 3C). Therefore, a simplistic assumption
379 would be that the addition of external Pi to cells in high glucose would also increase
380 mitochondrial Pi. However, an alternate possibility presents itself whererin since glycolytic
381 flux is already high in glucose, supplementing Pi will continue to fuel glycolysis. Indeed, this
382 was originally obseved by Harden and Young in 1908, where adding Pi increased fermentation
383 (Harden and Young, 1906). In such a scenario, there could be an increase in the cytosolic Pi
384 but not the mitochondrial Pi. We estimated the cytosolic and mitochondrial Pi in this
385 condition where excess Pi was externally supplemented. Notably, cells grown in high Pi had
386 increased cytosolic Pi, but decreased mitochondrial Pi (Figure 5-figure supplement 1C),
387 without any changes in total mitochondria volume or amounts (Figure 5-figure supplement
388 1D). Furthermore, directly adding Pi to cells growing in high glucose also decreased basal OCR
389 (Figure 5-figure supplement 1E), consistent with decreased mitochondrial Pi. These data

390 indicate that in high glucose, simply supplementing Pi will not increase Pi access to the
391 mitochondria, and instead results in an accumulation of Pi in the cytosol (Figure 5-figure
392 supplement 1C). We therefore now asked, if we inhibit glycolytic flux and then supplement
393 Pi, what would happen to mitochondrial activity. For this, we treated cells with 2DG, and
394 subsequently added Pi and measured the OCR (Figure 5-figure supplement 1F). In this case,
395 supplementing Pi increased the basal OCR (Figure 5-figure supplement 1F). Collectively, these
396 data suggest that a combination of decreasing glycolysis and increasing Pi can together
397 increase respiration. Next, in order to directly test mitochondrial activation based on external
398 Pi availability, we isolated mitochondria, and estimated activity *in vitro* upon adding
399 increasing Pi. Mitochondrial activity increased with increased Pi, with maximum activity
400 observed with 25 mM Pi supplemented (Figure 5D). In a complementary experiment, we
401 overexpressed the Mir1 transporter in wild-type cells, to increase Pi within mitochondria
402 (Figure 5-figure supplement 1G). Mir1-OE cells have higher Cox2 levels and basal OCR (Figure
403 5E, 5F). Therefore, increasing Pi transport to mitochondria is sufficient to increase
404 mitochondrial activity in high glucose.

405 Mitochondrial pyruvate transport is also required for mitochondrial respiration
406 (Timoń-Gómez et al., 2013). We asked where Pi availability stands in a hierarchy of constraints
407 for mitochondrial derepression, as compared to mitochondrial pyruvate transport. We
408 measured the amounts of the Mpc3 subunit of the mitochondrial pyruvate carrier (MPC)
409 complex (Bender et al., 2015; Timoń-Gómez et al., 2013). Mpc3 protein increases in *ubp3Δ*
410 (Figure 5-figure supplement 1H). This also correlated with the unimpaired TCA cycle flux
411 (Figure 2-figure supplement 2D) and the increased mitochondrial activity. Interestingly, in
412 *ubp3Δ* grown in low Pi, Mpc3 further increased (Figure 5-figure supplement 1H), but as shown
413 earlier this condition cannot increase OCR or mitochondrial activity (Figure 4F, Figure 4-figure
414 supplement 1F). Basal Mpc3 levels decrease in *mir1Δ*, but upon shifting to 0.1% glucose, Mpc3
415 increases in both WT and *mir1Δ*, with higher levels in *mir1Δ* (Figure 5-figure supplement 1I).
416 Therefore, even where Mpc3 is high (*ubp3Δ* in low Pi, and *mir1Δ* in low glucose),
417 mitochondrial activity remains low if Pi is restricted (Figure 4F, 4H). There was also no
418 decrease in basal OCR in *mpc3Δ* in high glucose, and the basal OCR increased to the same
419 level as of WT after shifting to 0.1% glucose (Figure 5-figure supplement 1J). Since Mpc3
420 changes with mitochondrial Pi availability (Figure S5G, S5H), we also measured Mpc3 in the

421 Mir1OE. No further changes in Mpc3 were observed in Mir1OE (Figure 5-figure supplement
422 1K), indicating that increasing mitochondrial Pi alone need not increase Mpc3. Overall,
423 although Mpc3 levels corelate with decreased glycolysis (*ubp3Δ* - Figure 5-figure supplement
424 1H, *ubp3Δ* in low Pi- Figure 5-figure supplement 1H, low glucose - Figure 5-figure supplement
425 1I), increased Mpc3 alone cannot increase mitochondrial activity and respiration in the
426 absence of adequate mitochondrial Pi.

427 Collectively, mitochondrial Pi availability constrains glucose-mediated mitochondrial
428 repression. Increasing available pools of Pi to enter the mitochondria is sufficient to induce
429 mitochondrial activity.

430 **Repression of mitochondrial respiration via Pi budgeting is conserved in Ubp3 mutants**
431 **across diverse yeast genetic backgrounds**

432 So far, we have identified a role for intracellular Pi budgeting as a constraint for
433 mitochondrial activity under high glucose. These were all carried out using a robust,
434 prototrophic yeast strain from a CEN.PK background. *S. cerevisiae* however, while Crabtree
435 positive, have tremendous genetic diversity (Peter et al., 2018). We therefore asked if this
436 mitochondrial repression through Pi budgeting (mediated by Ubp3 function) is conserved
437 across other strains of *S. cerevsiae* as well. To test this, we generated Ubp3 deletion mutants
438 in different genetic backgrounds of *S.* cerevsiae, including BY4742, W303 and Σ1278. In all
439 these strain backgrounds, we observed a significant increase in mitotracker fluorescne
440 intensity and Cox2 protein levels in *ubp3Δ* (Figure 6A, B). This suggests the role of Ubp3 as a
441 regulator of mitochondrial repression, independent of the genetic background of the yeast
442 (*S. cerevsiae*) strain. To further assess if loss of Ubp3 shows a concurrent increase in Pi levels,
443 we measured the total Pi levels in WT and *ubp3Δ* in a W303 strain background. We observed
444 a significant increase in total Pi levels in *ubp3Δ* cells in this strain (Figure 6C), similar to what
445 we observed in the CEN.PK strain (Figure 3C). Finally, to test if the altered Pi budgeting
446 regulates the mitochondrial activity in these cells, we measured the basal OCR in WT, *ubp3Δ*
447 and *ubp3Δ* in low (1 mM) Pi medium, in the W303 strain background. Consistent with the
448 increase in mitotracker fluorescence intensity and Cox2 protein levels, we observed a
449 significant increase in the basal OCR in *ubp3Δ* cells (Figure 6D). This increase was not observed
450 in *ubp3Δ* in a low Pi medium (Figure 6D). This suggests that the role of altered Pi budgeting in

451 regulating mitochondrial respiration is conserved in other genetic backgrounds of *S.*
452 *cerevisiae*.

453 Finally, we asked how important mitochondrial Pi transport was for growth, under
454 glycolytic inhibition. Consistent with the requirement for mitochondrial Pi transport to
455 increase mitochondrial respiration upon glycolytic inhibition (Figure 5B), WT cells only exhibit
456 a slightly decreased growth in the presence of 2DG (Figure 6E). In contrast, *mir1Δ* show a
457 severe growth defect upon 2DG treatment (Figure 6E), revealing a synergetic effect of
458 combining 2DG with inhibiting mitochondrial Pi transport. Therefore, the combined inhibition
459 of glycolysis and mitochondrial Pi transport restricts the growth of glycolytic cells.

460 Collectively, our data suggests a conserved role for intracellular Pi bugeting in
461 regulating mitochondrial repression in high glucose and the role of mitochondrial Pi transport
462 in regulating adaptation for growth under glycolytic inhibition.

463

464 **Discussion**

465 In this study, we highlight a role for Pi budgeting between cytosolic glycolysis and
466 mitochondrial processes (which compete for Pi) in constraining mitochondrial repression
467 (Figure 6F). Ubp3 controls this process (Figure 1), by maintaining the amounts of the glycolytic
468 enzymes Pfk1 and GAPDH (Tdh2 and Tdh3) and thereby allows high glycolytic flux. At high
469 fermentation rates, glycolytic enzymes levels at maximal activity maintain high glycolytic rates
470 (effectively following zero-order kinetics), and therefore, changes in the enzyme levels will
471 have a direct, proportionate effect on flux (Grigaitis and Teusink, 2022). The loss of Ubp3
472 decreases glycolytic flux, resulting in a systems-level, mass-action based rewiring of glucose
473 metabolism where more G6P is routed towards trehalose synthesis and PPP (Figure 2, Figure
474 6F). Indeed, inhibiting just phosphofructokinase can reroute glucose flux from glycolysis to
475 PPP (Hollinshead et al., 2016; Miyazawa et al., 2017; Yi et al., 2012), and our study now
476 permits contextualized interpretations of these results. Such reallocations of glucose flux will
477 collectively increase overall Pi, coming from the combined effect of increased Pi release from
478 trehalose synthesis, and decreased Pi consumption via reduced GAPDH. This altered
479 intracellular Pi economy increases Pi pools available to mitochondria, and increasing

480 mitochondrial Pi is necessary and sufficient to increase respiration in high glucose (Figure 4,
481 Figure 5, Figure 6). Mitochondrial Pi transport maintains mitochondrial activity in high
482 glucose, and increases mitochondrial activity in low glucose (Figure 4, Figure 5). Finally, the
483 mitochondrial Pi transporter Mir1 itself decreases in high glucose (Figure 5). Therefore, this
484 glucose-dependent repression of Mir1 also restricts mitochondrial Pi availability (and thereby
485 activity) in high glucose.

486 Traditionally, loss-of-function mutants of metabolic enzymes are used to understand
487 metabolic state regulation. This approach negates nuanced investigations, since metabolic
488 enzymes are often essential for viability. Furthermore, metabolic pathways have multiple,
489 contextually regulated nodes, through which cells maintain their metabolic state. Therefore,
490 alternate approaches to identify global regulators of metabolic states (as opposed to single
491 enzymes), might uncover ways via which multiple nodes are simultaneously tuned, and can
492 reveal unanticipated systems-level principles of metabolic state rewiring. In this study of
493 glucose-mediated mitochondrial repression, the loss of the DUB Ubp3 decreases glycolytic
494 flux by reducing the enzymes at two critical nodes in the pathway - Pfk1 and GAPDH. Unlike
495 loss of function mutants, a reduction in amounts will only rewire metabolic flux. By 'hitting'
496 multiple steps in glycolysis simultaneously, *ubp3Δ* have decreased Pi consumption, as well as
497 increased Pi release. Such a cumulative phenomenon reveals more than inhibiting only
498 GAPDH, where increased Pi comes only from reduced Pi consumption, and not from increased
499 trehalose biosynthesis. Our serendipitous identification of a regulator which regulates
500 multiple steps in glucose metabolism to change the metabolic environment, now suggests a
501 general basis of mitochondrial regulation that would have otherwise remained hidden.
502 Separately, finding the substrates of Ubp3 and whether Ubp3 directly regulates glycolytic
503 enzymes are exciting future research questions requiring concurrent innovations in accessible
504 chemical-biological approaches to study DUBs.

505 Because phosphates are ubiquitous, it is challenging to identify hierarchies of Pi-
506 dependent processes in metabolic state regulation (Gupta and Laxman, 2021). Phosphate
507 transfer reactions are the foundation of metabolism, driving multiple, thermodynamically
508 unfavorable reactions (Kamerlin et al., 2013; Westheimer, 1987). Contextually, the laws of
509 mass action predict that the relative rates of these reactions will regulate overall Pi balance,
510 and contrarily the Pi allocation to Pi-dependent reactions will determine reaction rates (Gupta

511 and Laxman, 2021; Van Heerden et al., 2014). Additionally, cells might control Pi allocations
512 for different reactions via compartmentalizing Pi in organelles, to spatially restrict Pi
513 availability (Booth and Guidotti, 1997; Solesio et al., 2021; Vila et al., 2022). Our data
514 collectively suggest a paradigm where the combination of factors regulates mitochondrial Pi
515 and thereby activity. In glycolytic yeast cells growing in high glucose, mitochondrial Pi
516 availability becomes restricted due to higher utilization of Pi in glycolysis compared to
517 mitochondria. Consistent with this, a rapid decrease in Pi upon glucose addition has been
518 observed (Hohmann et al., 1996; Koobs, 1972; Rodríguez-Enríquez et al., 2001). Interesting,
519 *in vitro* studies with isolated mitochondria from tumor cells also find that decreasing Pi levels
520 decreases respiration (Rodríguez-Enríquez et al., 2001), which would be consistent with this
521 scenario. Further, supplementing Pi correlates with decreased mitochondrial repression in
522 tumors (Brin and McKee, 1956; Koobs, 1972). By increasing Pi through a systems-level
523 rewiring of glucose metabolism (such as in *ubp3Δ* cells), cells can collectively increase
524 mitochondrial access to Pi. This Pi budgeting determines mitochondrial activity.
525 Supplementing Pi under conditions of low glycolysis (where mitochondrial Pi transport is
526 enhanced), as well as directly supplementing Pi to isolated mitochondria, increases
527 respiration (Figure 5, Figure 5-figure supplement 1). Notably, this increased respiration does
528 not happen upon directly supplementing Pi to highly glycolytic WT cells, where the Pi
529 increases in cytosol, without increasing mitochondrial Pi (Figure 5-figure supplement 1C).
530 Therefore, in order to derepress mitochondria, a combination of increased Pi along with
531 decreased glycolysis is required. An additional systems-level phenomenon that might regulate
532 Pi transport to the mitochondria is the decrease in cytosolic pH upon decreased glycolysis
533 (Dechant et al., 2010; Orij et al., 2011). The cytosolic pH in highly glycolytic cells is ~7, and
534 decreasing glycolysis results in cytosolic acidification (Dechant et al., 2010; Orij et al., 2011).
535 Therefore, under conditions of decreased glycolysis (2DG treatment, deletion of Ubp3, and
536 decreased GAPDH activity), cytosolic pH becomes acidic. Since mitochondrial Pi transport
537 itself is dependent on the proton gradient, a low cytosolic pH would favour mitochondrial Pi
538 transport (Hamel et al., 2004). Therefore, under conditions of decreased glycolysis (2DG
539 treatment, or loss of Ubp3, or decreased GAPDH activity), where cytosolic pH would be acidic,
540 increasing cytosolic Pi might indirectly increase mitochondria Pi transport, thereby leading to
541 increased respiration. Alternately, increasing mitochondrial Pi transporter amounts can
542 achieve the same result, as seen by overexpressing Mir1 (Figure 5). A similar observation has

543 been reported in *Arabidopsis*, reiterating an evolutionarily conserved role for mitochondrial
544 Pi in controlling respiration (Jia et al., 2015). Relatedly, glycolytic inhibition can suppress cell
545 proliferation in Warburg-positive tumors (O'Neill et al., 2019; Pelicano et al., 2006), or
546 inflammatory responses (Soto-Heredero et al., 2020). However, these cells survive by
547 switching to mitochondrial respiration (Lu et al., 2015; Shiratori et al., 2019), requiring
548 alternate approaches to prevent their proliferation (Cheng et al., 2012). Inhibiting
549 mitochondrial Pi transport in combination with glycolytic inhibition could restrict the
550 proliferation of Warburg/Crabtree positive cells. It is important to highlight that our
551 experiments, whether involving Pi supplementation or Pi limitations, maintain the cellular Pi
552 concentration within the millimolar range, and are conducted within a short timeframe (~ 1
553 hour). This differs significantly from Pi starvation studies, where cells are subjected to
554 prolonged and complete Pi deprivation. In those contexts, cells trigger extensive metabolic
555 adaptations in order to sustain available Pi pools including an increase in mitochondrial
556 membrane potential which can be independent of respiration (Ouyang et al., 2024).

557 Since its discovery in the 1920s, the phenomenon of accelerated glycolysis with
558 concurrent mitochondrial repression has been intensely researched. Yet, the biochemical
559 constraints for glucose-mediated mitochondrial repression remains unresolved. One
560 hypothesis suggests that the availability of glycolytic intermediates might determine the
561 extent of mitochondrial repression. F1,6BP inhibits complex III and IV of the electron transport
562 chain (ETC) in Crabtree positive yeast (Diaz-Ruiz et al., 2011; Díaz-Ruiz et al., 2008; Hammad
563 et al., 2016; Lemus et al., 2018). Similarly, the ratio between G6P and F1,6BP regulates the
564 extent of mitochondrial repression (Díaz-Ruiz et al., 2008; Lemus et al., 2018). Although
565 G6P/F6P accumulates in *ubp3Δ* (Figure 2C), this is not the case in *tdh2Δtdh3Δ* (GAPDH
566 mutant) (Figure 3-figure supplement 1D), suggesting that G6P/F6P accumulation in itself is
567 not the criterion to increase mitochondrial activity. Separately, the competition for common
568 metabolites/co-factors between glycolysis and respiration (such as ADP, Pi or pyruvate) could
569 drive this phenomenon (Diaz-Ruiz et al., 2011; Koobs, 1972). Here we observe that Mpc3
570 mediated mitochondrial pyruvate transport alone cannot increase respiration. An additional
571 consideration is the possible contribution of changes in ADP in regulating mitochondrial
572 activity, where the use of ADP in glycolysis might limit mitochondrial ADP. Therefore, when Pi
573 changes as a consequence of glycolysis, it coud be imagined that a change in ADP balance can

574 coincidentally occur. However, prior studies show that even though cytosolic ADP decreases
575 in the presence of glucose, this does not limit mitochondrial ADP uptake, or decrease
576 respiration, due to the very high affinity of the mitochondrial ADP transporter (Diaz-Ruiz et
577 al., 2011; Rodríguez-Enríquez et al., 2001). These collectively reiterate the importance of Pi
578 access and transport to mitochondria in constraining mitochondrial respiration. Indeed, this
579 interpretation can also contextually explain observations from other model systems where
580 mitochondrial Pi transport seems to regulate respiration (Scheibye-Knudsen and Quistorff,
581 2009; Seifert et al., 2015).

582 We parsimoniously suggest that Pi access to the mitochondria as a key constraint for
583 mitochondrial repression under high glucose. In a hypothetical scenario, a single-step event
584 in evolution, reducing mitochondrial Pi transporter amounts, and/or increasing glycolytic flux
585 (to deplete cytosolic Pi), will result in whole-scale metabolic rewiring to repress mitochondria.
586 More elaborate regulatory events can easily be imagined as subsequent adaptations to
587 enforce mitochondrial repression. Given the central role played by Pi, something as
588 fundamental as access to Pi will constrain mitochondrial repression. Concurrently, the rapid
589 incorporation of Pi into faster glycolysis can give cells a competitive advantage, while also
590 sequestering Pi in the form of usable ATP. Over the course of evolution, this could conceivably
591 drive other regulatory mechanisms to enforce mitochondrial repression, leading to the
592 currently observed complex regulatory networks and signaling programs observed in the
593 Crabtree effect, and other examples of glucose-dependent mitochondrial repression.

594

595 ## Materials and methods

596 ### Statistics and graphing

597 Unless otherwise indicated, statistical significance for all indicated experiments were
598 calculated using unpaired Student's t-tests (GraphPad prism 9.0.1). Graphs were plotted using
599 GraphPad prism 9.0.1

600 ### Yeast strains, media, and growth conditions

601 A prototrophic CEN.PK strain of *Saccharomyces cerevisiae* (WT) (J.P. van Dijken et al., 2000)
602 was used unless mentioned otherwise. Strains are listed in appendix table S1. Gene deletions,
603 chromosomal C-terminal tagged strains were generated by PCR mediated gene
604 deletion/tagging (Longtine et al., 1998). Mitochondria targeted Mneon strain (Mito-mNeon
605 green) is described in (Dua et al., 2022). The cox2-62 strain is described in (Bonnefoy et al.,
606 2001). Media compositions, growth conditions and CRISPR-Cas9 based mutagenesis are
607 described in extended methods (SI appendix).

608 **Mitotracker fluorescence**

609 Mitotracker fluorescence was measured using Thermo Varioscan™ LUX multimode plate
610 reader (579/599 excitation/emission). Detailed protocol is described in extended methods.
611 Mitotracker fluorescence were normalized using $OD_{600}$ of each sample and relative
612 fluorescence intensity calculated.

613 **Protein extraction and Western blotting**

614 Total protein was precipitated, extracted using trichloroacetic acid (TCA) as described earlier
615 (Vengayil et al., 2019). Blots were quantified using ImageJ software. Detailed protocol is
616 described in extended methods.

617 **Basal OCR measurement**

618 The basal OCR was measured using Agilent Seahorse XFe24 analyzer. Basal OCR readings were
619 normalized for cell number (using $OD_{600}$ of samples) in each well. The detailed methods are
620 described in extended methods.

621 **Mitochondrial volume estimation**

622 High-resolution 3D fluorescence experiments were performed on an inverted confocal laser
623 scanning microscope (Carl Zeiss LSM 780 or Olympus FV3000). For each imaging field of view,
624 sequential z-stacks were acquired for each excitation channel. 488 nm laser excitation for
625 mNeonGreen and 561 nm laser excitation for Mitotracker CMXros dye were used
626 respectively. Images taken were deconvolved and analyzed further in ImageJ software with
627 custom-written routines. Mitochondria segmentation and quantification was done using the

628 Mitochondria Analyzer plugin (Chaudhry et al., 2019) in Imagej. For visualization,
629 maximum intensity projection of 3D images was used.

630 **RNA extraction and RT-qPCR**

631 The RNA extraction was done using the hot phenol extraction method as described in
632 (Vengayil et al., 2019). The isolated RNA was DNase treated, and used for cDNA synthesis.
633 Superscript III reverse transcriptase enzyme (Invitrogen) was used for cDNA synthesis and RT-
634 qPCR was performed using KAPA SYBR FAST qRT PCR kit (KK4602, KAPA Biosystems). Taf10
635 was used as a control for normalisation and the fold change in mRNA levels were calculated
636 by 2^-ddct method.

637 **ATP, ethanol and Pi measurements**

638 ATP levels were measured by ATP estimation kit (Thermo Fisher A22066). Ethanol
639 concentration in the medium was estimated using potassium dichromate based assay
640 described in (Sriariyanun et al., 2019) with modifications. Pi was estimated using a malachite
641 green phosphate assay kit (Cayman chemicals, 10009325). Detailed sample collection and
642 assay protocols are described in extended methods.

643 **Metabolite extraction and analysis by LC-MS/MS**

644 The steady state levels and relative $^{13}C$ label incorporation into metabolites were estimated
645 by quantitative LC-MS/MS methods as described in (Walvekar et al., 2018). Detailed
646 methodology is extensively described in extended methods. Peak area measurements are
647 listed in supplement file 1.

648 **Mitochondrial isolation**

649 Mitochondria was isolated by immunoprecipitation as described in (Chen et al., 2017; Liao et
650 al., 2018) with modifications. The detailed protocol is described in extended methods (SI
651 appendix). The eluted mitochondria were used in malachite green assay for Pi estimation,
652 boiled with SDS-glycerol buffer for western blots or incubated with mitotracker CMXROS with
653 mitochondria-activation buffer for mitotracker assays.

654 **Cytosolic fraction isolation**

655 Cytosolic fraction was isolated from spheroplasts by centrifugation as described in detail in
656 S1 appendix. The total protein amounts in the cytosolic fraction was estimated by BCA protein
657 estimation assay and the Pi levels were estimated by malachite green assay.

658

659 **Data availability**

660 The LC-MS/MS peak area for all the metabolites can be found in supplement file 1. This study
661 includes no data deposited in external repositories.

662

663 **Acknowledgements**

664 We thank all SL lab members, Benjamin Tu, Anand Bachhawat and Vijay Jayaraman for
665 comments and suggestions. We acknowledge the NCBS/inStem/CCAMP mass spectrometry
666 facility for LC-MS/MS support. We thank Aayushee Khanna for help with experiments and
667 Gaurav Singh for help with microscopy. V.V acknowledges funding support from DST-INSPIRE
668 fellowship (IF170236) from the Department of Science and Technology (DST), Govt. of India,
669 S.N and SA acknowledges intramural funding from the DBT-inStem PhD program. S.L
670 acknowledges support from the DST SERB CRG grant CRG/2019/004772, a DBT-Wellcome
671 India Alliance Senior Fellowship (IA/S/21/2/505922), and institutional support from inStem.

672 **References**

673 Abdel-Haleem AM, Lewis NE, Jamshidi N, Mineta K, Gao X, Gojobori T. 2017. The emerging
674 facets of non-cancerous Warburg effect. *Front Endocrinol (Lausanne)* **8**:1–7.
675 doi:10.3389/fendo.2017.00279
676 Austin S, Mayer A. 2020. Phosphate Homeostasis − A Vital Metabolic Equilibrium
677 Maintained Through the INPHORS Signaling Pathway. *Front Microbiol* **11**:1367.
678 doi:10.3389/FMICB.2020.01367/BIBTEX
679 Bender T, Pena G, Martinou JJ-C. 2015. Regulation of mitochondrial pyruvate uptake by
680 alternative pyruvate carrier complexes. *EMBO J* **34**:1–14.
681 doi:10.15252/embj.201490197

682 Bonnefoy N, Bsat N, Fox TD. 2001. Mitochondrial Translation of Saccharomyces cerevisiae
683 COX2 mRNA Is Controlled by the Nucleotide Sequence Specifying the Pre-Cox2p Leader
684 Peptide. *Mol Cell Biol* **21**:2359–2372. doi:10.1128/MCB.21.7.2359
685 Booth JW, Guidotti G. 1997. Phosphate Transport in Yeast Vacuoles *. *J Biol Chem*
686 **272**:20408–20413. doi:10.1074/JBC.272.33.20408
687 Brazy PC, Mandel LJ, Dennis VW, Gullans SR. 1982. Metabolic Requirement for Inorganic
688 Phosphate by the Rabbit Proximal Tubule: EVIDENCE FOR A CRABTREE EFFECT
689 Metabolic Requirement for Inorganic Phosphate by the Rabbit Proximal Tubule
690 EVIDENCE FOR A CRABTREE EFFECT. *J Clin Invest* **70**:53. doi:10.1172/JCI110603
691 Brin M, McKee RW. 1956. The Inhibition of Respiration by Glucose, Fructose, and Mannose
692 in the Ehrlich Mouse Ascites Tumor. *Cancer Res* **16**:364–368.
693 Broach JR. 2012. Nutritional Control of Growth and Development in Yeast. *Genetics* **192**:73–
694 105. doi:10.1534/genetics.111.135731
695 Cai L, Tu BP. 2012. Driving the cell cycle through metabolism. *Annu Rev Cell Dev Biol* **28**:59–
696 87. doi:10.1146/annurev-cellbio-092910-154010
697 Chaudhry A, Shi R, Luciani XDS. 2019. INNOVATIVE METHODOLOGY A pipeline for
698 multidimensional confocal analysis of mitochondrial morphology , function , and
699 dynamics in pancreatic ℕ -cells. *Am J Physiol - Endocrinol Metab* **318**:87–101.
700 doi:10.1152/ajpendo.00457.2019
701 Chen WW, Freinkman E, Sabatini DM. 2017. Rapid immunopurification of mitochondria for
702 metabolite profiling and absolute quantification of matrix metabolites. *Nat Protoc*
703 **12**:2215. doi:10.1038/NPROT.2017.104
704 Cheng G, Zielonka J, Dranka BP, McAllister D, Mackinnon AC, Joseph J, Kalyanaraman B.
705 2012. Mitochondria-targeted drugs synergize with 2-deoxyglucose to trigger breast
706 cancer cell death. *Cancer Res* **72**:2634–2644. doi:10.1158/0008-5472.CAN-11-
707 3928/650337/AM/MITOCHONDRIA-TARGETED-DRUGS-SYNERGIZE-WITH-2
708 Cornish-Bowden A. 2016. Biochemical evolution : the pursuit of perfection, Garland science.
709 Crabtree HG. 1929. Observations on the carbohydrate metabolism of tumours. *Biochem J*
710 **23**:536–45. doi:10.1042/bj0230536
711 De Deken RH. 1966. The Crabtree effect: a regulatory system in yeast. *J Gen Microbiol*
712 **44**:149–56. doi:10.1099/00221287-44-2-149

713 Dechant R, Binda M, Lee SS, Pelet S, Winderickx J, Peter M. 2010. Cytosolic pH is a second
714 messenger for glucose and regulates the PKA pathway through V-ATPase. *EMBO J*
715 **29**:2515–2526.
716 Díaz-Ruiz R, Avéret N, Araiza D, Pinson B, Uribe-Carvajal S, Devin A, Rigoulet M. 2008.
717 Mitochondrial Oxidative Phosphorylation Is Regulated by Fructose 1,6-Bisphosphate: A
718 POSSIBLE ROLE IN CRABTREE EFFECT INDUCTION? *. *J Biol Chem* **283**:26948–26955.
719 doi:10.1074/JBC.M800408200
720 Diaz-Ruiz R, Rigoulet M, Devin A. 2011. The Warburg and Crabtree effects: On the origin of
721 cancer cell energy metabolism and of yeast glucose repression. *Biochim Biophys Acta -*
722 *Bioenerg* **1807**:568–576. doi:10.1016/j.bbabio.2010.08.010
723 Dua N, Seshadri A, Badrinarayanan A. 2022. DarT-mediated mtDNA damage induces
724 dynamic reorganization and selective segregation of mitochondria. *J Cell Biol* **221**.
725 Fontanesi F, Soto IC, Horn D, Barrientos A. 2006. Assembly of mitochondrial cytochrome c-
726 oxidase, a complicated and highly regulated cellular process. *Am J Physiol - Cell Physiol*
727 **291**:1129–1147.
728 doi:10.1152/AJPCELL.00233.2006/ASSET/IMAGES/LARGE/ZH00110649540005.JPEG
729 Grigaitis P, Teusink B. 2022. An excess of glycolytic enzymes under glucose-limited
730 conditions may enable Saccharomyces cerevisiae to adapt to nutrient availability. *FEBS*
731 *Lett*. doi:10.1002/1873-3468.14484
732 Gupta R, Laxman S. 2021. Cycles, sources, and sinks: Conceptualizing how phosphate
733 balance modulates carbon flux using yeast metabolic networks. *Elife* **10**:1–14.
734 doi:10.7554/elife.63341
735 Gupta R, Walvekar AS, Liang S, Rashida Z, Shah P, Laxman S. 2019. A tRNA modification
736 balances carbon and nitrogen metabolism by regulating phosphate homeostasis. *Elife*
737 **8**. doi:10.7554/eLife.44795
738 Hamel P, Saint-Georges Y, De Pinto B, Lachacinski N, Altamura N, Dujardin G. 2004.
739 Redundancy in the function of mitochondrial phosphate transport in Saccharomyces
740 cerevisiae and Arabidopsis thaliana. *Mol Microbiol* **51**:307–317. doi:10.1046/j.1365-
741 2958.2003.03810.x
742 Hammad N, Rosas-Lemus M, Uribe-Carvajal S, Rigoulet M, Devin A. 2016. The Crabtree and
743 Warburg effects: Do metabolite-induced regulations participate in their induction?
744 *Biochim Biophys Acta - Bioenerg* **1857**:1139–1146. doi:10.1016/j.bbabio.2016.03.034

745 Harden A, Young WJ. 1906. The alcoholic Ferment of Yeast-juice.Part III.-The Function of
746 Phosphates in the Fermentation o f Glucose hy Yeast-juice. *Proc R Soc London Ser B,*
747 **77**:405.
748 Hershko A, Ciechanover A. 1998. THE UBIQUITIN SYSTEM. *Annu Rev Biochem* **67**:425–79.
749 Hitosugi T, Chen J. 2014. Post-translational modifications and the Warburg effect. *Oncogene*
750 **33**:4279–4285. doi:10.1038/onc.2013.406
751 Hohmann S, Bell W, Neves MJ, Valckx D, Thevelein JM. 1996. Evidence for trehalose-6-
752 phosphate-dependent and-independent mechanisms in the control of sugar influx into
753 yeast glycolysis. *Mol Microbiol* **20**:981–991. doi:10.1111/j.1365-2958.1996.tb02539.x
754 Hollinshead WD, Rodriguez S, Martin HG, Wang G, Baidoo EEK, Sale KL, Keasling JD,
755 Mukhopadhyay A, Tang YJ. 2016. Examining Escherichia coli glycolytic pathways,
756 catabolite repression, and metabolite channeling using Δpfk mutants. *Biotechnol*
757 *Biofuels* **9**:1–13. doi:10.1186/s13068-016-0630-y
758 Hunter T. 2012. Why nature chose phosphate to modify proteins. *Philos Trans R Soc B Biol*
759 *Sci* **367**:2513–2516. doi:10.1098/RSTB.2012.0013
760 Isasa M, Rose CM, Elsasser S, Navarrete-Perea J, Paulo JA, Finley DJ, Gygi SP. 2015.
761 Multiplexed, Proteome-Wide Protein Expression Profiling: Yeast Deubiquitylating
762 Enzyme Knockout Strains. *J Proteome Res* **14**:5306–5317.
763 doi:10.1021/acs.jproteome.5b00802
764 J.P. van Dijken JB, Brambillac L, Dubocd P, Francoise JM, Gancedof C, Giusepping,
765 M.L.F.HEijnenh JJ, Hoarei M, Langej HC, Maddenk EA, Niederbergerb P, Nielsend, J., J.L.
766 Parroue , T. Petitf , D. Porroc MR, Rielg N van, Rizzij M, H.Y. Steensmaa, k , C.T.
767 Verripsg, J. Vindeløvd, Pronka JT. 2000. An interlaboratory comparison of physiological
768 and genetic properties of four Saccharomyces cerevisiae strains. *Enzyme Microb*
769 *Technol* **26**:706–714.
770 Jia F, Wan X, Zhu W, Sun D, Zheng C, Liu P, Huang J. 2015. Overexpression of Mitochondrial
771 Phosphate Transporter 3 Severely Hampers Plant Development through Regulating
772 Mitochondrial Function in Arabidopsis. *PLoS One* **10**:e0129717.
773 doi:10.1371/JOURNAL.PONE.0129717
774 Kamerlin SCLL, Sharma PK, Prasad RB, Warshel A. 2013. Why nature really chose phosphate.
775 *Q Rev Biophys* **46**:1–132. doi:10.1017/S0033583512000157
776 Komander D, Rape M. 2012. The Ubiquitin Code. *Annu Rev Biochem* **81**:203–229.

777 doi:10.1146/annurev-biochem-060310-170328
778 Koobs DH. 1972. Phosphate mediation of the Crabtree and Pasteur effects. *Science (80- )*
779 **178**:127–133. doi:10.1126/science.178.4057.127
780 Kornberg MD. 2020. The immunologic Warburg effect: Evidence and therapeutic
781 opportunities in autoimmunity. *Wiley Interdiscip Rev Syst Biol Med* **12**:1–17.
782 doi:10.1002/wsbm.1486
783 Lemus MR, Roussarie E, Hammad N, Mougeolle A, Ransac S, Issa R, Mazat JP, Uribe-Carvajal
784 S, Rigoulet M, Devin A. 2018. The role of glycolysis-derived hexose phosphates in the
785 induction of the Crabtree effect. *J Biol Chem* **293**:12843–12854.
786 doi:10.1074/JBC.RA118.003672
787 Liao PC, Boldogh IR, Siegmund SE, Freyberg Z, Pon LA. 2018. Isolation of mitochondria from
788 Saccharomyces cerevisiae using magnetic bead affinity purification. *PLoS One* **13**:1–15.
789 doi:10.1371/journal.pone.0196632
790 Ljungdahl POO, Daignan-Fornier B. 2012. Regulation of Amino Acid, Nucleotide, and
791 Phosphate Metabolism in Saccharomyces cerevisiae. *Genetics* **190**:885–929.
792 doi:10.1534/genetics.111.133306
793 Longtine MS, McKenzie A, Demarini DJ, Shah NG, Wach A, Brachat A, Philippsen P, Pringle
794 JR. 1998. Additional modules for versatile and economical PCR-based gene deletion and
795 modification in Saccharomyces cerevisiae. *Yeast* **14**:953–961. doi:10.1002/(SICI)1097-
796 0061(199807)14:10<953::AID-YEA293>3.0.CO;2-U
797 Lu CL, Qin L, Liu HC, Candas D, Fan M, Li JJ. 2015. Tumor Cells Switch to Mitochondrial
798 Oxidative Phosphorylation under Radiation via mTOR-Mediated Hexokinase II Inhibition
799 - A Warburg-Reversing Effect. *PLoS One* **10**:e0121046.
800 doi:10.1371/JOURNAL.PONE.0121046
801 Mason PW, Carbone DP, Cushman RA, Waggoner AS. 1981. The importance of inorganic
802 phosphate in regulation of energy metabolism of Streptococcus lactis. *J Biol Chem*
803 **256**:1861–1866. doi:10.1016/S0021-9258(19)69886-8
804 Miyazawa H, Yamaguchi Y, Sugiura Y, Honda K, Kondo K, Matsuda F, Yamamoto T, Suematsu
805 M, Miura M. 2017. Rewiring of embryonic glucose metabolism via suppression of PFK-1
806 and aldolase during mouse chorioallantoic branching. *Dev* **144**:63–73.
807 doi:10.1242/dev.138545
808 Mouillon JM, Persson BL. 2006. New aspects on phosphate sensing and signalling in

809 Saccharomyces cerevisiae. *FEMS Yeast Res* **6**:171–176. doi:10.1111/j.1567-
810 1364.2006.00036.x
811 Murakami H, Blobel G, Pain D. 1990. Isolation and characterization of the gene for a yeast
812 mitochondrial import receptor. *Nat 1990 3476292* **347**:488–491.
813 doi:10.1038/347488a0
814 Nelson DL (David L, Nelson DL (David L, Lehninger AL, Cox MM. 2008. Lehninger principles of
815 biochemistry.
816 Nostramo R, Varia SN, Zhang B, Emerson MM, Herman PK. 2016. The Catalytic Activity of the
817 Ubp3 Deubiquitinating Protease Is Required for Efficient Stress Granule Assembly in
818 Saccharomyces cerevisiae. *Mol Cell Biol* **36**:173. doi:10.1128/MCB.00609-15
819 O'Neill S, Porter RK, McNamee N, Martinez VG, O'Driscoll L. 2019. 2-Deoxy-D-Glucose
820 inhibits aggressive triple-negative breast cancer cells by targeting glycolysis and the
821 cancer stem cell phenotype. *Sci Rep* **9**:1–11. doi:10.1038/s41598-019-39789-9
822 Orij R, Brul S, Smits GJ. 2011. Intracellular pH is a tightly controlled signal in yeast. *Biochim*
823 *Biophys Acta - Gen Subj* **1810**:933–944. doi:10.1016/j.bbagen.2011.03.011
824 Ossareh-Nazari B, Bonizec M, Cohen M, Dokudovskaya S, Delalande F, Schaeffer C, Van
825 Dorsselaer A, Dargemont C. 2010. Cdc48 and Ufd3, new partners of the ubiquitin
826 protease Ubp3, are required for ribophagy. *EMBO Rep* **11**:548–554.
827 doi:10.1038/embor.2010.74
828 Ouyang Y, Jeong M-Y, Cunningham CN, Berg JA, Toshniwal AG, Hughes CE, Seiler K, Van
829 Vranken JG, Cluntun AA, Lam G, Winter JM, Akdogan E, Dove KK, Nowinski SM, West M,
830 Odorizzi G, Gygi SP, Dunn CD, Winge DR, Rutter J. 2024. Phosphate starvation signaling
831 increases mitochondrial membrane potential through respiration-independent
832 mechanisms. *Elife* **13**:e84282. doi:10.7554/eLife.84282
833 Pacini N, Borziani F. 2014. Cancer stem cell theory and the warburg effect, two sides of the
834 same Coin? *Int J Mol Sci* **15**:8893–8930. doi:10.3390/ijms15058893
835 Pelicano H, Martin DS, Xu RH, Huang P. 2006. Glycolysis inhibition for anticancer treatment.
836 *Oncogene 2006 2534* **25**:4633–4646. doi:10.1038/sj.onc.1209597
837 Peter J, De Chiara M, Friedrich A, Yue J-X, Pflieger D, Bergström A, Sigwalt A, Barre B, Freel K,
838 Llored A, Cruaud C, Labadie K, Aury J-M, Istace B, Lebrigand K, Barbry P, Engelen S,
839 Lemainque A, Wincker P, Liti G, Schacherer J. 2018. Genome evolution across 1,011
840 Saccharomyces cerevisiae isolates. *Nature* **556**:339–344. doi:10.1038/s41586-018-

841 0030-5
842 Pickart CM, Eddins MJ. 2004. Ubiquitin: structures, functions, mechanisms. *Biochem Biophys*
843 *Acta* **1695**:55–72.
844 Postma E, Verduyn C, Scheffers WA, Van Dijken JP. 1989. Enzymic analysis of the crabtree
845 effect in glucose-limited chemostat cultures of Saccharomyces cerevisiae. *Appl Environ*
846 *Microbiol* **55**:468–77.
847 Rodríguez-Enríquez S, Juárez O, Rodríguez-Zavala JS, Moreno-Sánchez R. 2001. Multisite
848 control of the Crabtree effect in ascites hepatoma cells. *Eur J Biochem* **268**:2512–2519.
849 doi:10.1046/j.1432-1327.2001.02140.x
850 Scheibye-Knudsen M, Quistorff B. 2009. Regulation of mitochondrial respiration by inorganic
851 phosphate; comparing permeabilized muscle fibers and isolated mitochondria
852 prepared from type-1 and type-2 rat skeletal muscle. *Eur J Appl Physiol* **105**:279–287.
853 doi:10.1007/s00421-008-0901-9
854 Seifert EL, Ligeti E, Mayr JA, Sondheimer N, Hajnóczky G. 2015. The mitochondrial
855 phosphate carrier: Role in oxidative metabolism, calcium handling and mitochondrial
856 disease. *Biochem Biophys Res Commun* **464**:369–375. doi:10.1016/J.BBRC.2015.06.031
857 Shestov AA, Liu X, Ser Z, Cluntun AA, Hung YP, Huang L, Kim D, Le A, Yellen G, Albeck JG,
858 Locasale JW. 2014. Quantitative determinants of aerobic glycolysis identify flux through
859 the enzyme GAPDH as a limiting step. *Elife* **3**:1–18. doi:10.7554/ELIFE.03342
860 Shiratori R, Furuichi K, Yamaguchi M, Miyazaki N, Aoki H, Chibana H, Ito K, Aoki S. 2019.
861 Glycolytic suppression dramatically changes the intracellular metabolic profile of
862 multiple cancer cell lines in a mitochondrial metabolism-dependent manner. *Sci Rep*
863 **9**:1–15. doi:10.1038/s41598-019-55296-3
864 Solesio ME, Xie L, McIntyre B, Ellenberger M, Mitaishvili E, Bhadra-Lobo S, Bettcher LF, Bazil
865 JN, Raftery D, Jakob U, Pavlov E V. 2021. Depletion of mitochondrial inorganic
866 polyphosphate ( polyP) in mammalian cells causes metabolic shift from oxidative
867 phosphorylation to glycolysis. *Biochem J* **478**:1631–1646. doi:10.1042/BCJ20200975
868 Soto-Heredero G, Gómez de las Heras MM, Gabandé-Rodríguez E, Oller J, Mittelbrunn M.
869 2020. Glycolysis – a key player in the inflammatory response. *FEBS J* **287**:3350–3369.
870 doi:10.1111/FEBS.15327
871 Sriariyanun M, Mutrakulcharoen P, Tepaamorndech S, Cheenkachorn K, Rattanaporn K.
872 2019. A Rapid Spectrophotometric Method for Quantitative Determination of Ethanol

873 in Fermentation Products. *Orient J Chem* **35**:744–750. doi:10.13005/OJC/350234
874 Timoń-Gómez A, Proft M, Pascual-Ahuir A. 2013. Differential Regulation of Mitochondrial
875 Pyruvate Carrier Genes Modulates Respiratory Capacity and Stress Tolerance in Yeast.
876 *PLoS One* **8**:e79405. doi:10.1371/JOURNAL.PONE.0079405
877 Tripodi F, Nicastro R, Reghellin V, Coccetti P. 2015. Post-translational modifications on yeast
878 carbon metabolism: Regulatory mechanisms beyond transcriptional control. *Biochim*
879 *Biophys Acta - Gen Subj* **1850**:620–627. doi:10.1016/j.bbagen.2014.12.010
880 Tsogtbaatar E, Landin C, Minter-Dykhouse K, Folmes CDL. 2020. Energy Metabolism
881 Regulates Stem Cell Pluripotency. *Front Cell Dev Biol* **8**:1–16.
882 doi:10.3389/fcell.2020.00087
883 Van Heerden JH, Wortel MT, Bruggeman FJ, Heijnen JJ, Bollen YJM, Planqué R, Hulshof J,
884 O'Toole TG, Wahl SA, Teusink B. 2014. Lost in transition: Start-up of glycolysis yields
885 subpopulations of nongrowing cells. *Science (80- )* **343**. doi:10.1126/science.1245114
886 Vander Heiden MG, Cantley LC, Thompson CB. 2009. Understanding the Warburg Effect: The
887 Metabolic Requirements of Cell Proliferation. *Science (80- )* **324**:1029–1033.
888 Vengayil V, Rashida Z, Laxman S. 2019. The E3 ubiquitin ligase Pib1 regulates effective
889 gluconeogenic shutdown upon glucose availability. *J Biol Chem*.
890 doi:10.1074/jbc.RA119.009822
891 Vila T, Frases S, Gomesid FM. 2022. Lessons from protozoans: Phosphate sensing and
892 polyphosphate storage in fungi. *PLOS Pathog* **18**:e1010298.
893 doi:10.1371/JOURNAL.PPAT.1010298
894 Walvekar A, Rashida Z, Maddali H, Laxman S. 2018. A versatile LC-MS/MS approach for
895 comprehensive, quantitative analysis of central metabolic pathways. *Wellcome Open*
896 *Res* **3**:122. doi:10.12688/wellcomeopenres.14832.1
897 Warburg O. 1925. The Metabolism of Carcinoma Cells. *Cancer Res* **9**:148–163.
898 Westheimer FH. 1987. Why Nature Chose Phosphates. *Science (80- )* **235**:1173–1178.
899 doi:10.1126/SCIENCE.2434996
900 Xia L, Oyang L, Lin J, Tan S, Han Y, Wu N, Yi P, Tang L, Pan Q, Rao S, Liang J, Tang Y, Su M, Luo
901 X, Yang Y, Shi Y, Wang H, Zhou Y, Liao Q. 2021. The cancer metabolic reprogramming
902 and immune response. *Mol Cancer* **20**:1–21. doi:10.1186/s12943-021-01316-8
903 Yi W, Clark PM, Mason DE, Keenan MC, Hill C, Goddard WA, Peters EC, Driggers EM, Hsieh-
904 Wilson LC. 2012. PFK1 Glycosylation Is a Key Regulator of Cancer Cell Growth and

905 Central Metabolic Pathways. *Science* **337**:975. doi:10.1126/SCIENCE.1222278
906 Zara V, Dietmeier K, Palmisano A, Vozza A, Rassow J, Palmieri F, Pfanner N. 1996. Yeast
907 mitochondria lacking the phosphate carrier/p32 are blocked in phosphate transport
908 but can import preproteins after regeneration of a membrane potential. *Mol Cell Biol*
909 **16**:6524–6531. doi:10.1128/mcb.16.11.6524
910 Zhu J, Thompson CB. 2019. Metabolic regulation of cell growth and proliferation. *Nat Rev*
911 *Mol Cell Biol* **20**:436–450. doi:10.1038/s41580-019-0123-5
912
913

914 **Figure legends**

915 **Figure 1: A deubiquitinase deletion screen identifies Ubp3 as a regulator of glucose-**
916 **mediated mitochondrial repression**

917 A) Schematic depicting glucose-mediated mitochondrial repression (Crabtree effect).

918 B) Schematic describing the screen with a yeast DUB KO library to identify regulators of
919 Crabtree effect.

920 C) Identifying DUB knockouts with altered mitochondrial potential. Heat map shows relative
921 mitochondrial membrane potential of 19 deubiquitinase deletions in high glucose, from 2
922 biological replicates. Also see figure 1-figure supplements 1A, B.

923 D) The deubiquitinase activity of Ubp3 and repression of mitochondrial membrane potential.
924 WT, *ubp3Δ,* and Ubp3$^{C469A}$ were grown in high glucose and relative mitochondrial membrane
925 potential was measured. Data represent mean ± SD from three biological replicates (n=3).
926 Also see figure 1-figure supplement 1 D.

927 E) Effect of loss of Ubp3 on ETC complex IV subunit Cox2. WT and *ubp3Δ* were grown in high
928 glucose, and Cox2 was measured (western blot using an anti-Cox2 antibody). A representative
929 blot (out of 3 biological replicates, n=3) and their quantifications are shown. Data represent
930 mean ± SD.

931 F) Basal oxygen consumption rate (OCR) in high glucose in *ubp3Δ*. WT and *ubp3Δ* were grown
932 in high glucose, and OCR was measured. Basal OCR corresponding to ~3 x 10^5 cells, from two
933 independent experiments (n=2), normalized to the $OD_{600}$ is shown. Bar graph representations
934 are shown in the inset. Data represent mean ± SD.

935 G) Total ATP levels in *ubp3Δ* and WT. WT and *ubp3Δ* were grown in high glucose, and total
936 ATP were measured. Data represent mean ± SD from three biological replicates (n=3).

937 H) Dependence of *ubp3Δ* on mitochondrial ATP. WT and *ubp3Δ* cells were grown in high
938 glucose, and treated with 1 mM sodium azide for 45 minutes. Total ATP levels in sodium azide
939 treated and untreated cells were measured. Data represent mean ± SD (n=3).

940 I) Requirement for mitochondrial respiration in high glucose in *ubp3Δ*. A growth curve of WT
941 and *ubp3Δ* in high glucose in the presence of OXPHOS uncoupler FCCP (10 µM), and serial
942 dilution growth assay in high glucose in the presence/absence of sodium azide (1 mM) are
943 shown. Data represent mean ± SD (n=2). Also see figure 1-figure supplement 1 H, I.

944 Data information: **p<0.01, ***p<0.001.

945

946 **Figure 2: Key glycolytic enzymes decrease and glucose flux is rerouted in *ubp3Δ* cells**

947 A) A schematic illustrating directions of glucose-6-phosphate (G6) flux in cells. Glucose is
948 converted to G6P, a precursor for trehalose, the pentose phosphate pathway (PPP), and
949 glycolysis.

950 B) Effect of loss of Ubp3 on key glycolytic enzymes. WT and *ubp3Δ* were grown in high glucose
951 and the Pfk1, Tdh2, and Tdh3 levels were measured by western blot using an anti-FLAG
952 antibody. A representative blot (out of three biological replicates, n=3) and their
953 quantification are shown. Data represent mean ± SD. Also see figure 2-figure supplement 1A.

954 C) Steady-state metabolite amounts in WT and *ubp3Δ* in high glucose. Relative steady-state
955 levels of trehalose, major glycolytic, and PPP intermediates were estimated in WT and *ubp3Δ*.
956 Data represent mean ± SD from three biological replicates (n=3). Also see Appendix Table S3.

957 D) Relative glycolytic and trehalose synthesis flux in WT and *ubp3Δ*. Relative $^{13}C$-label
958 incorporation into trehalose and glycolytic intermediates, after a pulse of 1% $^{13}C_6$ glucose is
959 shown. Data represent mean ± SD from three biological replicates (n=3). Also see Appendix
960 Table S3, figure 2-figure supplement 1 D, E.

961 E) Ethanol production in *ubp3Δ*. WT and *ubp3Δ* were grown in high glucose and ethanol in the
962 media was measured. Data represent mean ± SD from three biological replicates (n=3).

963 F) Relative rate of ethanol production in WT vs *ubp3Δ*. WT and *ubp3Δ* were grown in high
964 glucose (to $OD_{600}$ ~ 0.6), equal numbers of cells were shifted to fresh medium (high glucose)
965 and ethanol concentration in the medium was measured temporally. Data represent mean ±
966 SD from three biological replicates (n=3)

967 Data information: *p<0.05, **p<0.01, ***p<0.001.

968

969 **Figure 3: Rerouted glucose flux results in phosphate (Pi) accumulation**

970 A) Changes in protein levels in *ubp3Δ* (dataset from Isasa et al., 2015). *ubp3Δ* cells have an
971 increase in proteins involved in mitochondrial respiration and decrease in proteins involved
972 in glucose and phosphate metabolism.

973 B) Schematic showing maintenance of Pi balance during glycolysis. Trehalose synthesis from
974 G6P releases Pi, and the conversion of G3P to 1,3BPG by GAPDH consumes Pi. In *ubp3Δ*,
975 trehalose biosynthesis (which releases Pi) increases. *ubp3Δ* have decreased GAPDH, which
976 will decrease Pi consumption. This increase in Pi release along with decreased Pi consumption
977 could increase cytosolic Pi.

978 C) Intracellular Pi levels in WT and *ubp3Δ*. WT and *ubp3Δ* were grown in high glucose and the
979 total free phosphate (Pi) levels were estimated. WT in high Pi (2% glucose, 10mM Pi) was a
980 positive control. Data represent mean ± SD from three biological replicates (n=3). Also see
981 figure 3-figure supplement 1A.

982 D) Pho regulon responses in WT and *ubp3Δ*. Protein levels of Pho84-FLAG and Pho12-FLAG
983 were compared between WT grown in high glucose and in high Pi, *ubp3Δ* in high glucose with
984 or without a shift to a no-Pi medium for one hour, by western blot. A representative blot (out
985 of three biological replicates, n=3) and their quantifications are shown. Data represent mean
986 ± SD.

987 E) Contribution of trehalose synthesis as a Pi source. WT, *tps2Δ*, *ubp3Δ,* and *ubp3Δtps2Δ* were
988 grown in high glucose and the total Pi levels were estimated. Data represent mean ± SD from
989 three biological replicates (n=3). Also see figure 3-figure supplement 1B.

990 F) Loss of GAPDH isozymes Tdh2 and Tdh3 and effect on Pi. WT, *ubp3Δ,* and *tdh2Δtdh3Δ* were
991 grown in high glucose and total Pi was estimated. Data represent mean ± SD from three
992 biological replicates (n=3).

993 G) Pi levels in *ubp3Δ* and *tdh2Δtdh3Δ* cells in ethanol medium. WT, *ubp3Δ,* and *tdh2Δtdh3Δ*
994 cells were grown in ethanol medium and the total Pi levels were estimated. Data represent
995 mean ± SD from three biological replicates (n=3).

996 Data information: *p<0.05, **p<0.01, ***p<0.001, ****p<0.0001.

997

998 **Figure 4: Mitochondrial Pi availability correlates with mitochondrial activity in *ubp3Δ***

999 A) A hypothetical mechanism of cytosolic free Pi controling mitochondrial activity by
1000 regulating mitochondrial Pi availability.

1001 B) Cytosolic and mitochondrial Pi amounts in WT vs *ubp3Δ*. The cytosolic fraction was isolated
1002 by centrifugation (see SI appendix), and in separate experiments, mitochondria were isolated
1003 by immunoprecipitation from WT and *ubp3Δ* and mitochondrial Pi estimated. (i) Cytosolic Pi
1004 levels (relative as well as absolute) and (ii) mitochondrial Pi levels (normalised to Idh1) are
1005 shown. Data represent mean ± SD from three biological replicates (n=3) respectively for the
1006 cytosolic and mitochondrial measurements. Also see figure 4-figure supplement 1A, B.

1007 C) Cox2 protein in *tdh2Δtdh3Δ*. WT, *ubp3Δ,* and *tdh2Δtdh3Δ* were grown in high glucose and
1008 Cox2 protein was estimated. A representative blot (out of three biological replicates, n=3) and
1009 their quantifications are shown. Data represent mean ± SD.

1010 D) Basal OCR levels in *tdh2Δtdh3Δ*. WT, *ubp3Δ,* and *tdh2Δtdh3Δ* were grown in high glucose
1011 and basal OCR was measured from two independent experiments (n=2). Data represent mean
1012 ± SD. Also see figure 4-figure supplement 1C.

1013 E) Comparative Pi amounts and Cox2 levels in *ubp3Δ*, *tdh2Δtdh3Δ,* WT cells. WT cells were
1014 grown in high glucose, *ubp3Δ* and *tdh2Δtdh3Δ* were grown in high glucose and low Pi, and
1015 Cox2 protein was estimated. A representative blot (out of three biological replicates, n=3) and
1016 their quantifications are shown. Data represent mean ± SD. Also see figure figure 4-figure
1017 supplement 1D, F.

1018 F) Pi amounts and basal OCR in *ubp3Δ* and *tdh2Δtdh3Δ* vs WT cells. WT cells were grown in
1019 high glucose, *ubp3Δ* and *tdh2Δtdh3Δ* were grown in high glucose and low Pi, and basal OCR
1020 was measured from three independent experiments (n=3). Data represent mean ± SD.

1021 G) Effect of loss of mitochondrial Pi transporter Mir1 on Cox2protein. WT, *ubp3Δ*, *mir1Δ,* and
1022 *mir1Δubp3Δ* were grown in high glucose and Cox2 amounts compared. A representative blot
1023 (out of three biological replicates, n=3) and their quantifications are shown. Data represent
1024 mean ± SD.

1025 H) Relationship of mitochondrial Pi transport and basal OCR in WT vs *ubp3Δ*. WT, *ubp3Δ*,
1026 *mir1Δ,* and *mir1Δubp3Δ* cells were grown in high glucose and basal OCR was measured from
1027 two independent experiments (n=2). Data represent mean ± SD.

1028 Data information: *p<0.05, **p<0.01, ****p<0.0001.

1029

1030 **Figure 5: Mitochondrial Pi availability constrains mitochondrial activity under high glucose**

1031 A) Relationship of mitochondrial Pi transport and respiration after glucose removal. WT and
1032 *mir1Δ* cells were cultured in high (2%) glucose and shifted to low (0.1%) glucose for 1 hour.
1033 The normalized basal OCR, from two independent experiments (n=2) are shown. Data
1034 represent mean ± SD.

1035 B) Requirement of mitochondrial Pi transport for switch to respiration upon glycolytic
1036 inhibition by 2DG. WT and *mir1Δ* cells were cultured in high glucose and treated with or
1037 without 0.25% 2DG for 1 hour. Basal OCR was measured from two independent experiments
1038 (n=2). Data represent mean ± SD. Also see figure 5-figure supplement 1A.

1039 C) Glucose-dependent regulation of Mir1. Cells (with Mir1-HA) were grown in high glucose
1040 and shifted to low glucose (0.1% glucose) for 1 hour, and Mir1 levels compared. A
1041 representative blot (out of three biological replicates, n=3) and their quantifications are
1042 shown. Data represent mean ± SD. Also see figure 5-figure supplement 1B.

1043 D) Increasing Pi concentrations and mitochondrial activity in isolated mitochondria.
1044 Mitochondria were isolated from WT cells grown in high glucose, incubated with 1 mM

1045 pyruvate, 1 mM malate, 0.5 mM ADP and 0-50 mM $KH_2PO_4$. The mitochondrial activity was
1046 estimated by mitotracker fluorescence intensity, and intensities relative to the sample with 0
1047 mM $KH_2PO_4$ is shown. Data represent mean ± SD from three biological replicates (n=3).

1048 E) Effect of overexpressing Mir1 on Cox2 protein. WT (containing empty vector) and Mir1
1049 overexpressing (Mir1OE) cells were grown in high glucose and Cox2 levels were estimated. A
1050 representative blot (out of three biological replicates, n=3) and their quantifications are
1051 shown. Data represent mean ± SD. Also see figure S5F.

1052 F) Effect of overexpressing Mir1 on basal OCR. The basal OCR in WT (containing empty vector)
1053 and Mir1OE in high glucose was measured from three independent experiments (n=3). Data
1054 represent mean ± SD.

1055 Data information: *p<0.05, **p<0.01, ***p<0.001.

1056

1057 **Figure 6: Repression of mitochondrial respiration via Pi budgeting is conserved in Ubp3**
1058 **mutants across diverse yeast genetic backgrounds**

1059 A) Effect of loss of Ubp3 on mitochondrial membrane potential in different yeast strains. WT
1060 and *ubp3Δ* cells (in CEN.PK, BY4742, W303 and Σ1278 strains of *S. cerevisiae*) were grown in
1061 high glucose and relative mitochondrial membrane potential was measured. Data represent
1062 mean ± SD from three biological replicates (n=3).

1063 B) Effect of loss of Ubp3 on ETC complex IV subunit Cox2. WT and *ubp3Δ* (in BY4742, W303
1064 and Σ1278 strains of *S. cerevisiae*) were grown in high glucose, and Cox2 was measured. A
1065 representative blot (out of 3 biological replicates, n=3) and their quantifications are shown.
1066 Data represent mean ± SD.

1067 C) Intracellular Pi levels in WT and *ubp3Δ* in W303 strain background. WT and *ubp3Δ* (in W303
1068 strain background) were grown in high glucose and the total free phosphate (Pi) levels were
1069 estimated. Data represent mean ± SD from three biological replicates (n=3).

1070 D) Effect of low Pi on the basal OCR in WT and *ubp3Δ* cells in W303 strain background. WT
1071 cells were grown in high glucose and *ubp3Δ* were grown in high glucose and low Pi, and basal
1072 OCR was measured. Data represent mean ± SD (n=3).

1073 E) Requirement of mitochondrial Pi transport for growth after 2DG treatment. Shown are
1074 serial dilution growth assays in high glucose in the presence and absence of 0.1% 2DG, using
1075 WT and *mir1Δ* cells. The results after 40hrs incubation/30°C are shown.

1076 F) A model illustrating how mitochondrial Pi availability controls mitochondrial activity. In high
1077 glucose, the decreased Pi due to high Pi consumption in glycolysis, along with the glucose-
1078 mediated repression of mitochondrial Pi transporters, decreases mitochondrial Pi availability.
1079 This reduces mitochondrial activity. In low glucose, increased mitochondrial Pi transporters
1080 and lower glycolytic flux increases mitochondrial Pi, leading to enhanced mitochondrial
1081 activity. In *ubp3Δ* cells in high glucose, high trehalose synthesis and lower glycolytic flux
1082 results in an increase in Pi. This increases mitochondrial Pi availability and thereby the
1083 mitochondrial activity.

1084 Data information: *p<0.05, **p<0.01, ***p<0.001.

1085

1086

1087

1088

1089

1090

1091

1092

1093

1094 ## Supplement figure legends

1095 **Figure 1-figure supplement 1: DUB screen details and further characterization of Ubp3**
1096 **functions**

1097 A) A list of the known/identified *S. cerevisiae* deubiquitinase enzymes is shown. The DUBs
1098 which were used in this study, and the mitotracker intensity of two biological replicates (n=2)
1099 relative to WT are shown.

1100 B) WT cells grown in a respiratory, ethanol medium and mitotracker fluorescence intensity
1101 compared to glucose medium. WT cells were grown in high glucose medium (2% glucose) and
1102 ethanol medium (2% ethanol), and the mitochondrial membrane potential was measured.
1103 Data from two independent experiments (n=2) is shown. Data represent mean ± SD.

1104 C) Representative images of WT and *ubp3Δ* cells treated with mitotracker red CMXROS.

1105 D) Schematic representation of the conserved domains of Ubp3 and its mammalian ortholog
1106 Usp10. The catalytic cysteine of Usp10 and Ubp3 is highlighted.

1107 E) The catalytically inactive mutant of Ubp3, Ubp3$^{C469A}$ does not have altered Ubp3 protein
1108 levels. WT and Ubp3$^{C469A}$ cells containing endogenous Ubp3 tagged with 3xFLAG (C terminus)
1109 were grown in high glucose and the protein levels of Ubp3 were measured. A representative
1110 blot (out of three biological replicates, n=3) and their quantification are shown. Data
1111 represent mean ± SD.

1112 F) The total mitochondrial volume does not change in *ubp3Δ* cells. WT and *ubp3Δ* cells with
1113 mitochondria targeted mNeon green were imaged, and the total mitochondrial volume per
1114 cell (n=104 for WT, n=107 for *ubp3Δ*) was calculated. A representative image and
1115 quantification are shown. Data represent mean ± SD.

1116 G) Tom70 protein amounts do not change in *ubp3Δ* cells. WT and *ubp3Δ* cells containing
1117 endogenous Tom70 tagged at the C terminus with a 3xFLAG epitope were grown in high
1118 glucose and the protein levels of Tom70 were measured by western blot. A representative
1119 blot (out of three biological replicates, n=3) and their quantification are shown. Data
1120 represent mean ± SD.

1121 H) Dependence of *ubp3Δ* on mitochondrial respiration. WT and *ubp3Δ* cells were grown in
1122 high glucose with or without mitochondrial inhibitor oligomycin (25 µM), and the $OD_{600}$ was
1123 measured at different time points. Data represent mean ± SD (n=2).

1124 I) Dependence of *ubp3Δ* on functional mitochondrial respiration. Ubp3 deletions were done
1125 in respiration defective strains -Rho0, cox2-62, *atp1Δ* and *atp10Δ*, and serial dilution growth
1126 assay was done in high glucose. The results after 24 hours of incubation at 30°C are shown.

1127 J) Changes in global ubiquitination state in WT and *ubp3Δ.* WT and *ubp3Δ* cells were grown in
1128 high glucose with or without heat stress (42°C/1 hour), and the changes in global total
1129 ubiquitination was estimated by western blotting using an anti-ubiquitin antibody.

1130

1131 **Figure 2-figure supplement 1: Further estimates of glycolytic enzymes and flux**

1132 A) Loss of Ubp3 does not change the protein levels of enolase isozymes Eno1 and Eno2. WT
1133 and *ubp3Δ* cells containing Eno1 and Eno2 C terminus endogenously tagged with a 3x FLAG
1134 epitope, were grown in high glucose and protein amounts were estimated. A representative
1135 blot (out of three biological replicates, n=3) is shown in the lower panel, quantifications
1136 shown in the upper panel. Data represent mean ± SD.

1137 B) The decreased levels of glycolytic enzymes in *ubp3Δ* cells is not because of proteasomal
1138 degradation. WT and *ubp3Δ* were grown in high glucose and *ubp3Δ* cells were treated with
1139 or without MG132 (100 µM) for 30 minutes. Pfk1, Tdh2, and Tdh3 levels were measured by
1140 western blot using an anti-FLAG antibody. A representative blot (out of three biological
1141 replicates, n=3) and their quantification are shown. Data represent mean ± SD.

1142 C) Loss of Ubp3 results in decreased transcription of PFK1, TDH2 and TDH3 genes. WT, *ubp3Δ*
1143 and $Ubp3^{C469A}$ cells were grown in high glucose and the mRNA levels of PFK1, TDH2 and TDH3
1144 were analysed by RT-qPCR. The fold changes in mRNA levels are shown. Data represent mean
1145 ± SD.

1146 D) Steady-state pyruvate levels in WT and *ubp3Δ* in high glucose. Data represent mean ± SD
1147 from three biological replicates (n=3). Also see Appendix Table S3.

1148 E) Schematic showing the experimental design for measuring $^{13}C$ label incorporation into
1149 glycolytic intermediates and trehalose using a $^{13}C_6$ glucose-pulse.

1150 F) Changes in $^{13}C$ label incorporation into glycolytic intermediates and trehalose with time,
1151 and linearity of label incorporation after a pulse of 1% $^{13}C_6$ glucose is shown.

1152

1153 **Figure 2- figure supplement 2: Estimation of steady state levels and flux of TCA cycle**
1154 **intermediates**

1155 A) Steady-state TCA metabolite amounts in WT and *ubp3Δ* in high glucose. Relative steady-
1156 state levels of TCA cycle intermediates were estimated in WT and *ubp3Δ*. Data represent
1157 mean ± SD from three biological replicates (n=3). Also see Appendix Table S3.

1158 B) Schematic showing the experimental design for measuring $^{13}C$ label incorporation into TCA
1159 cycle intermediates using a $^{13}C_6$ glucose-pulse.

1160 C) Changes in $^{13}C$ label incorporation into TCA cycle intermediates with time, and linearity of
1161 label incorporation after a pulse of 1% $^{13}C_6$ glucose is shown.

1162 D) Relative TCA cycle flux in WT and *ubp3Δ*. Relative $^{13}C$-label incorporation into TCA cycle
1163 intermediates, after a pulse of 1% $^{13}C_6$ glucose is shown. Data represent mean ± SD from three
1164 biological replicates (n=3). Also see Appendix Table S3.

1165 Data information: *p<0.05

1166

1167 **Figure 3-figure supplement 1: Comparisons of phosphate, ethanol and other metabolites in**
1168 **WT, *ubp3Δ* and GAPDH mutants**

1169 A) Loss of Ubp3 deubiquitinase activity and Pi levels. WT, *ubp3Δ,* and $Ubp3^{C469A}$ cells were
1170 grown in high glucose and the total free phosphate (Pi) levels were estimated. Data from two
1171 independent experiments (n=2) is shown. Data represent mean ± SD. B) Trehalose levels in
1172 WT and *ubp3Δ* cells in the absence of Tps2. *tps2Δ* and *ubp3Δtps2Δ* cells were grown in high

1173 glucose, and the trehalose levels were estimated using targeted LC-MS/MS. Data represent
1174 mean ± SD from three biological replicates (n=3).

1175 C) Loss of GAPDH isozymes Tdh2 and Tdh3 and ethanol production. WT and *tdh2Δtdh3Δ* cells
1176 were grown in high glucose and the ethanol concentration in the medium was measured.
1177 Data are represented as mean ± SD from three biological replicates (n=3). Note: The WT
1178 shown here is same as the WT in Figure 2E, the ethanol assays in Figure 2E and Figure S3C
1179 were done together and a common WT control was used.

1180 D) Steady state levels of glycolytic intermediates: *tdh2Δtdh3Δ* cells have unaltered steady
1181 state levels of G6P/F6P, increased levels of F1,6 BP and G3P and decreased levels of 3PG and
1182 PEP. WT and *tdh2Δtdh3Δ* cells were grown in high glucose and the steady state amounts of
1183 glycolytic intermediates were estimated using targeted LC-MS/MS. Data represent mean ± SD
1184 from three biological replicates (n=3). Also see Appendix Table S3.

1185 E) Trehalose levels in *tdh2Δtdh3Δ* cells. WT and *tdh2Δtdh3Δ* cells were grown in high glucose
1186 and trehalose amounts were estimated using targeted LC-MS/MS. Data represent mean ± SD
1187 from three biological replicates (n=3).

1188 Data information: *p<0.05, **p<0.01.

1189

1190 **Figure 4-figure supplement 1: Mitochondrial Pi estimation characterizations and**
1191 **correlations of mitochondrial activity with Pi availability**

1192 A) Isolation of cytosolic fraction by centrifugation and lack of vacuolar contamination in
1193 mitochondria isolated by immunoprecipitation. Cytosolic fraction was isolated from WT cells
1194 grown in high glucose with or without excess Pi and *ubp3Δ* cells. Eno1 was used as a cytosolic
1195 marker and Cox2 as mitochondrial marker to ensure purity of the cytosolic fractions.
1196 Mitochondria were isolated from WT cells grown in high glucose and the protein levels of
1197 Tom20, Cox2, Idh1 and Vph1 and were measured in cell lysate and immunoprecipitated
1198 mitochondria by western blot.

1199 B) Idh1 levels in *ubp3Δ* cells and WT cells grown in high Pi. WT cells were grown in high
1200 glucose, or high glucose and high Pi medium (10mM Pi) and *ubp3Δ* cells were grown in high
1201 glucose, and the Idh1 protein levels were estimated by western blot. A representative blot
1202 (out of three biological replicates, n=3) is shown in the lower panel. Quantification is shown
1203 in the upper panel. Data represent mean ± SD.

1204 C) Mitochondrial membrane potential in *tdh2Δtdh3Δ* cells. WT, *ubp3Δ,* and *tdh2Δtdh3Δ* cells
1205 were grown in high glucose and the mitochondrial membrane potential was measured. Data
1206 represent mean ± SD from three biological replicates (n=3).

1207 D) Pi levels in *ubp3Δ* cells grown in low Pi (1mM Pi) vs WT cells. WT cells were grown in high
1208 glucose and *ubp3Δ* cells were grown in high glucose or high glucose-low Pi, and the total Pi
1209 levels were estimated. Data represent mean ± SD from three biological replicates (n=3).

1210 E) Ethanol production in *ubp3Δ* cells grown in a low Pi medium. WT cells were grown in high
1211 glucose and *ubp3Δ* cells were grown in high glucose or high glucose-low Pi, and the ethanol
1212 concentration in the medium was measured. Data represent mean ± SD from three biological
1213 replicates (n=3).

1214 F) Pi amounts and mitochondrial membrane potential in WT, *ubp3Δ,* and *tdh2Δtdh3Δ* cells.
1215 The cells were grown in high glucose or high glucose-low Pi, and the mitochondrial membrane
1216 potential was measured. Data from two independent experiments (n=2) is shown. Data
1217 represent mean ± SD.

1218 G) The Pi mediated change in basal OCR in *ubp3Δ* is dependent on mitochondrial respiration.
1219 WT and Rho0 cells were grown in high glucose, Rho0/*ubp3Δ* were grown in high glucose and
1220 low Pi, and basal OCR was measured from three independent experiments (n=3). Data
1221 represent mean ± SD.

1222 H) The protein levels of mitochondrial Pi transporters Mir1 and Pic2 in *ubp3Δ* cells. WT and
1223 *ubp3Δ* cells containing endogenously tagged Mir1 and Pic2 at their C terminus with a 6x HA
1224 epitope tag were grown in high glucose and Mir1 and Pic2 proteins were measured by
1225 western blot. A representative blot (out of three biological replicates, n=3) is shown in the
1226 lower panel. Quantification is shown in the upper panel. Data represent mean ± SD.

1227 Data information: *p<0.05, **p<0.01, ***p<0.001.

1228

1229 **Figure 5-figure supplement 1: Mitochondrial phosphate and pyruvate transport**
1230 **relationships with mitochondrial activity**

1231 A) Requirement of Mir1 for switching to increased mitochondrial activity upon 2-
1232 deoxyglucose (2-DG) treatment. WT and *mir1Δ* cells were grown in high glucose and treated
1233 with 0.1% and 0.25% 2-DG for one hour. The mitochondrial membrane potential was
1234 measured from two independent experiments (n=2). Data represent mean ± SD.

1235 B) Mir1 protein levels and glucose repression. Cells containing Mir1 endogenously tagged at
1236 the C terminus with a 6x HA epitope tag were grown in high glucose or a respiratory medium
1237 (2% ethanol). Mir1 protein was estimated by western blot. A representative blot (out of three
1238 biological replicates, n=3) is shown in the lower panel. Quantification is shown in the upper
1239 panel. Data represent mean ± SD.

1240 C) Effect of supplementing Pi in the medium on cytosolic and mitochondrial Pi. WT cells were
1241 grown in high glucose, and high glucose-high Pi medium (10 mM Pi). The cytosolic fraction
1242 was isolated by centrifugation (see SI appendix), and in separate experiments, mitochondria
1243 were isolated by immunoprecipitation from WT and *ubp3Δ* and mitochondrial Pi estimated.
1244 (i) Cytosolic Pi levels (relative and absolute) and (ii) mitochondrial Pi levels normalised to Idh1
1245 protein levels is shown. Data represent mean ± SD from three biological replicates (n=3). Also
1246 see figure 4-figure supplement 1A, B.

1247 D) Effect of supplementing Pi on the total mitochondrial volume. WT cells with mitochondria
1248 targeted mNeon green were grown in high glucose, and high glucose, high Pi medium (10 mM
1249 Pi), cells were imaged and the total mitochondrial volume per cell was calculated.

1250 E) Increasing Pi concentration in a high glucose medium results in a decrease in basal OCR.
1251 WT cells were grown in high glucose medium (YPD-Pi medium), supplemented with 5 mM Pi
1252 and at $OD_{600}$~0.6, the medium was supplemented with Pi (10 mM and 25 mM final
1253 concentrations). The basal OCR was measured one hour after Pi supplementation. Data
1254 represent mean ± SD from three biological replicates (n=3).

1255 E) Effect of increasing the Pi concentration in a high glucose medium, in the presence of 2DG,
1256 on basal OCR. WT cells were grown in high glucose medium (YPD-Pi medium), supplemented
1257 with 5 mM Pi and at $OD_{600}$~0.6, the medium was supplemented with Pi (25 mM final
1258 concentration) and 2DG (0.25%) for one hour and the basal OCR was measured. Data
1259 represent mean ± SD from three biological replicates (n=3).

1260 F) Overexpression of Mir1. C terminal 6x HA epitope-tagged Mir1 was expressed under G6PD
1261 promoter in cells with Mir1 endogenously tagged at the C terminus with a 6x-HA epitope tag.
1262 WT cells (carrying an empty vector, and expressing Mir1-HA under the endogenous Mir1
1263 promoter) and Mir1-OE cells were grown in high glucose. The protein levels of Mir1 were
1264 estimated by western blot, and clones with an ~2-fold increase in Mir1 were selected. A
1265 representative blot (out of three biological replicates, n=3) is shown in the lower panel.
1266 Quantification is shown in the upper panel. Data represent mean ± SD.

1267 G) Mpc3 protein levels in *ubp3Δ* cells. WT and *ubp3Δ* cells containing endogenously tagged
1268 Mpc3 at the C terminus with a 3x FLAG epitope tag, were cultured in high glucose (2% glucose)
1269 and high glucose-low Pi (2% glucose, 1 mM Pi). The Mpc3 protein levels were measured by
1270 western blot. A representative blot (out of three biological replicates, n=3) is shown in the
1271 lower panel, quantifications shown in the upper panel. Data represent mean ± SD.

1272 H) Mpc3 protein amounts upon shifting WT and *mir1Δ* cells to a low-glucose medium. WT and
1273 *mir1Δ* cells containing Mpc3-FLAG, were cultured in high glucose (2% glucose) and shifted to
1274 low (0.1%) glucose for 1 hour. Mpc3 protein was measured by western blot. A representative
1275 blot (out of three biological replicates, n=3) is shown in the lower panel, quantifications
1276 shown in the upper panel. Data represent mean ± SD.

1277 I) Requirement of Mpc3 for the increase in basal OCR upon shifting to low glucose. WT and
1278 *mpc3Δ* cells were cultured in high glucose (2% glucose) and shifted to low (0.1%) glucose for
1279 1 hour. The basal OCR from two independent experiments (n=2), normalized to the $OD_{600}$ is
1280 shown. Data represent mean ± SD.

1281 J) Mpc3 levels and Mir1 overexpression. WT cells and Mir1-OE cells containing endogenously
1282 tagged Mpc3 ate the C terminus with a 3x FLAG tag were grown in high glucose. The protein
1283 levels of Mpc3 were estimated by western blot. A representative blot (out of three biological

1284 replicates, n=3) is shown in the panel. Quantification is shown in the upper panel. Data
1285 represent mean ± SD. Data information: *p<0.05, **p<0.01, ***p<0.001.

Figure 1: A deubiquitinase deletion screen identifies Ubp3 as a regulator of glucose-mediated mitochondrial repression

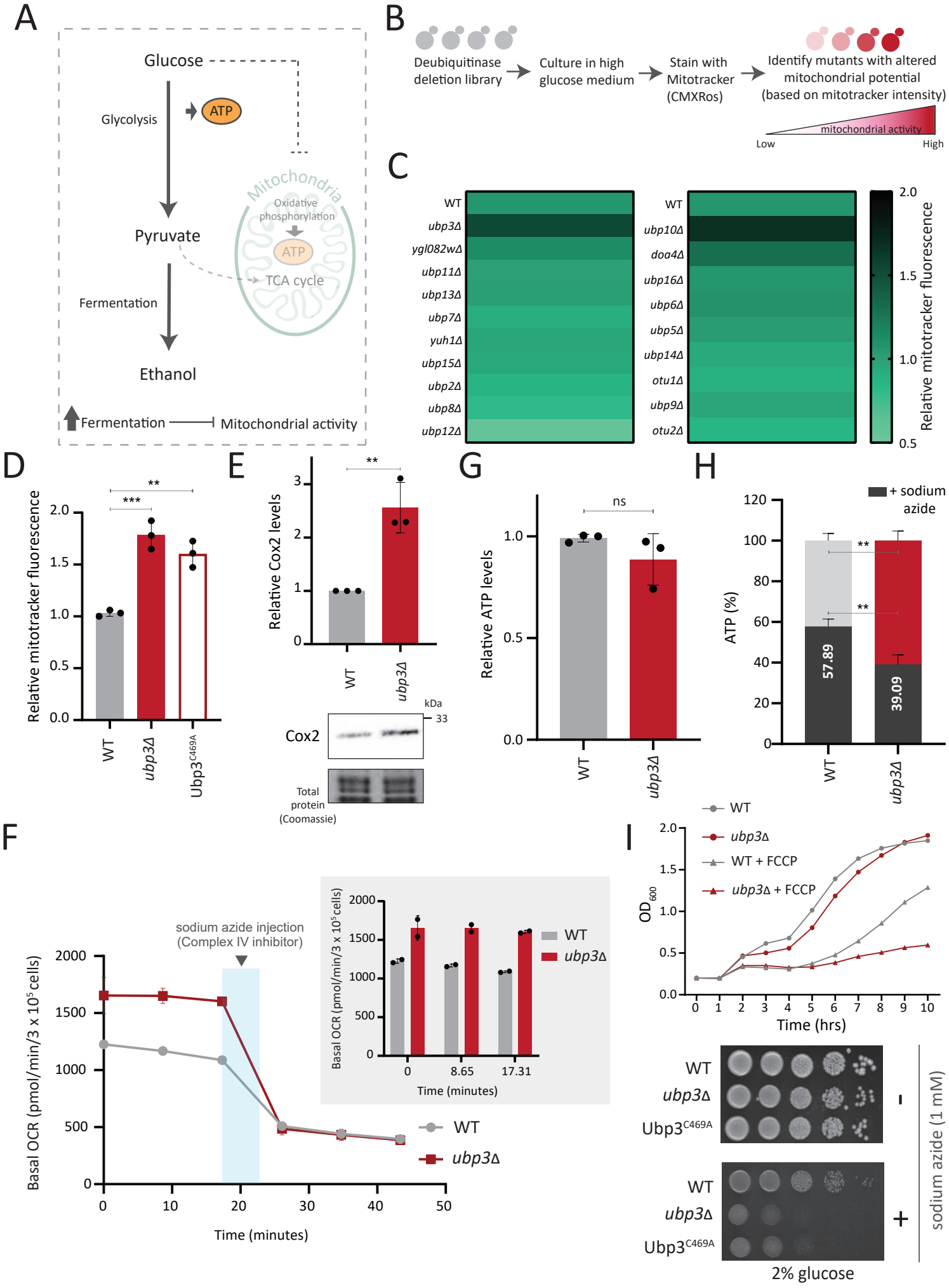

Figure 2: Key glycolytic enzymes decrease and glucose flux is rerouted in *ubp3Δ* cells

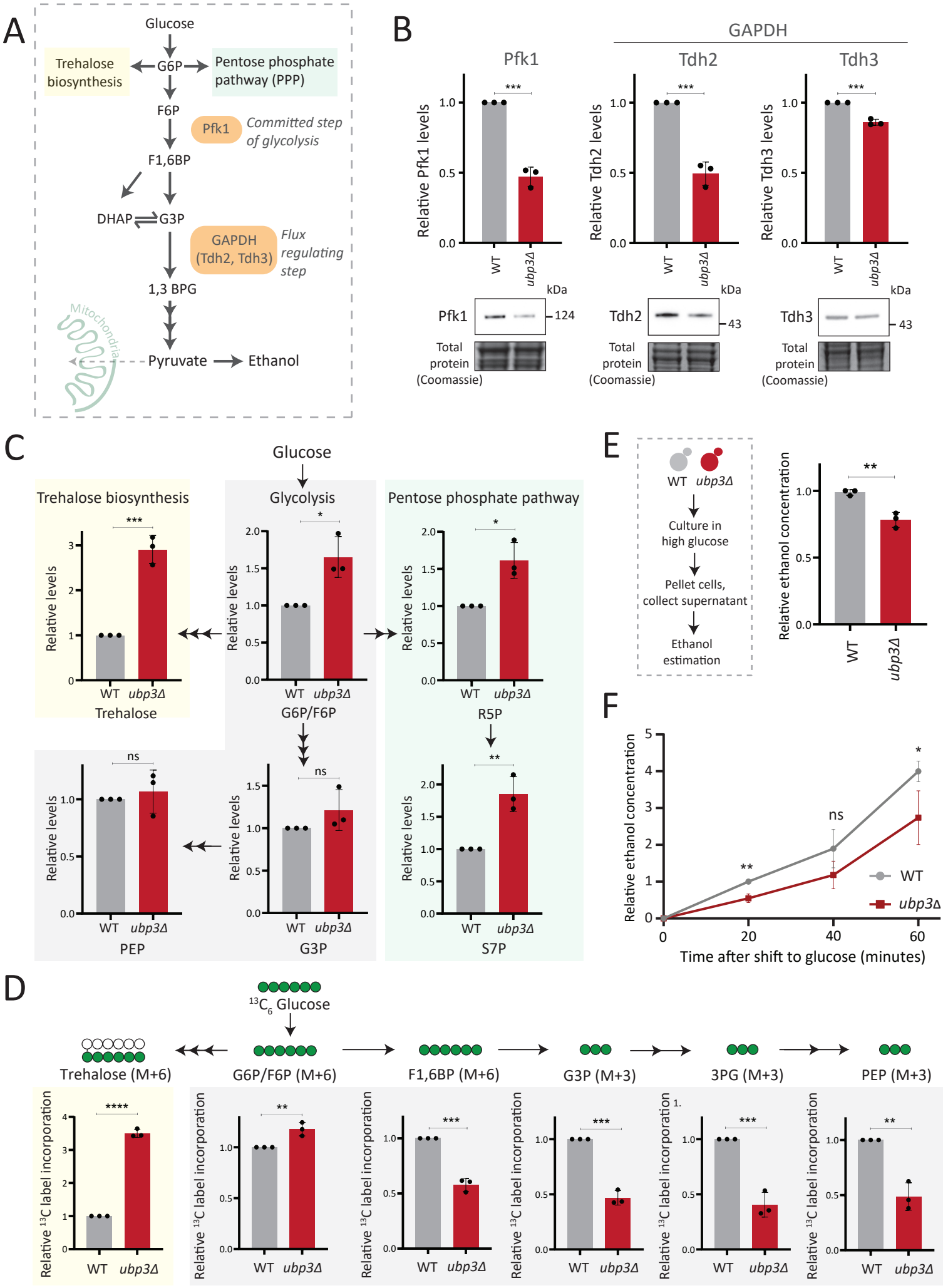

Figure 3: Rerouted glucose flux results in phosphate (Pi) accumulation

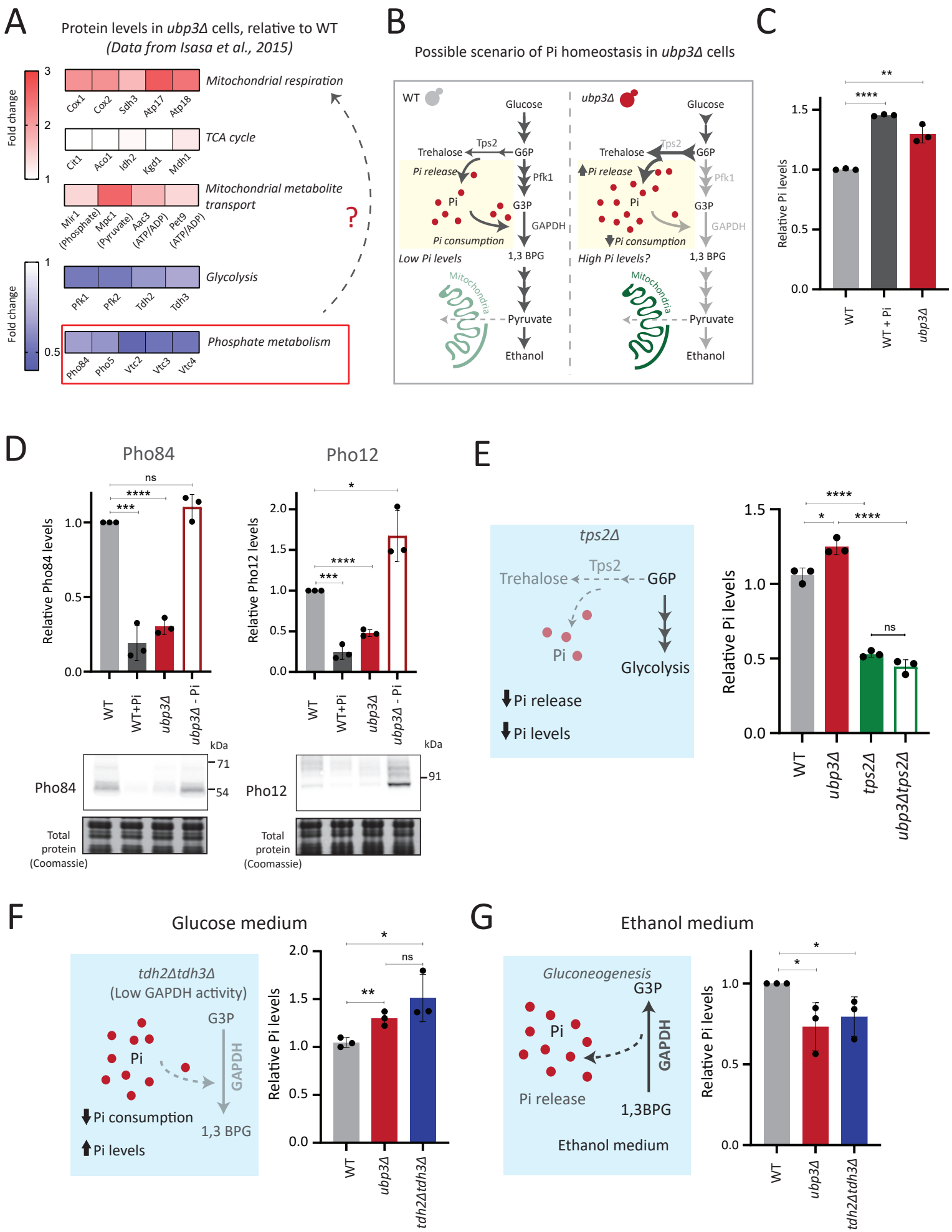

Figure 4: Mitochondrial Pi availability correlates with mitochondrial activity in *ubp3Δ*

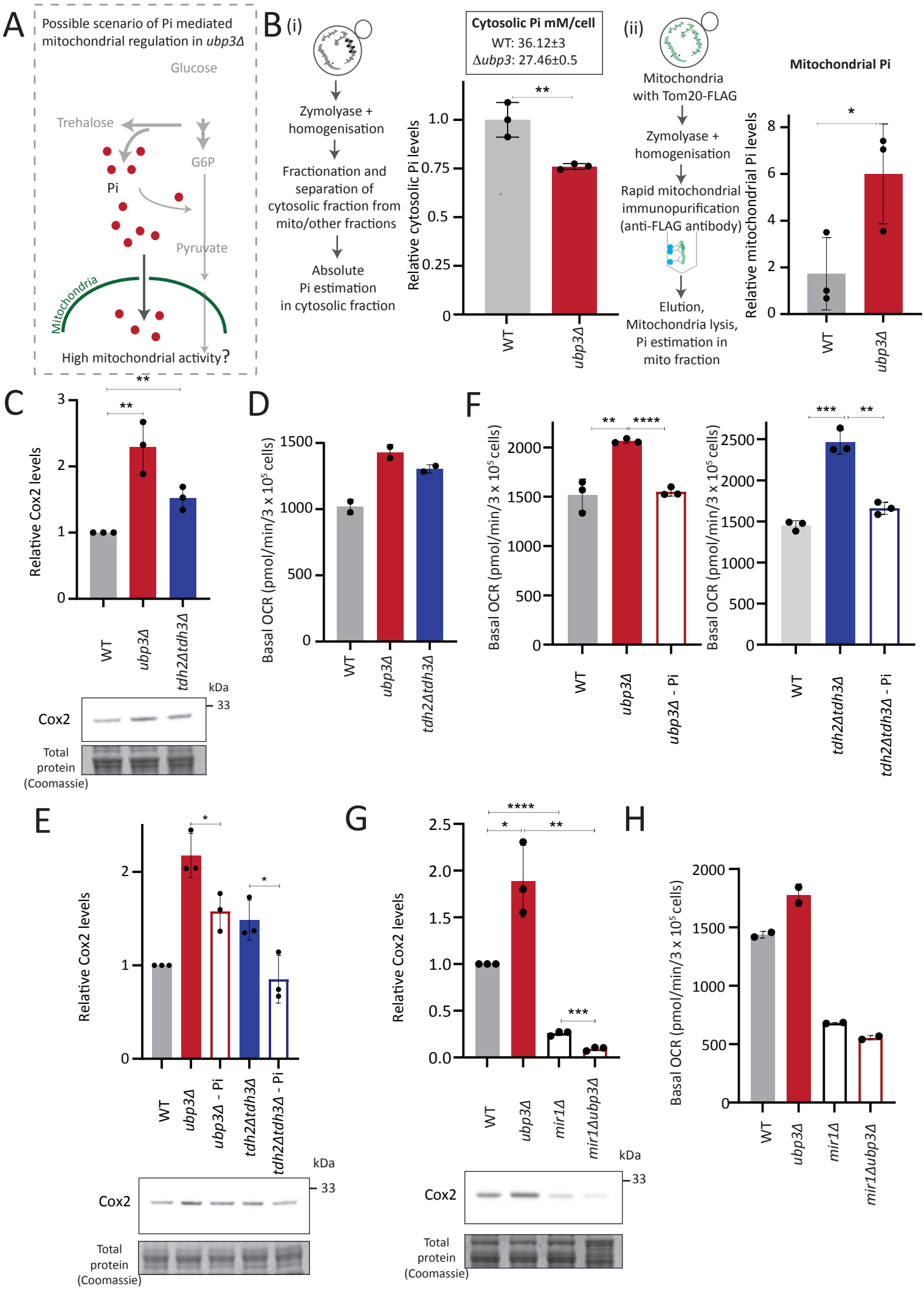

Figure 5: Mitochondrial Pi availability constrains mitochondrial activity under high glucose

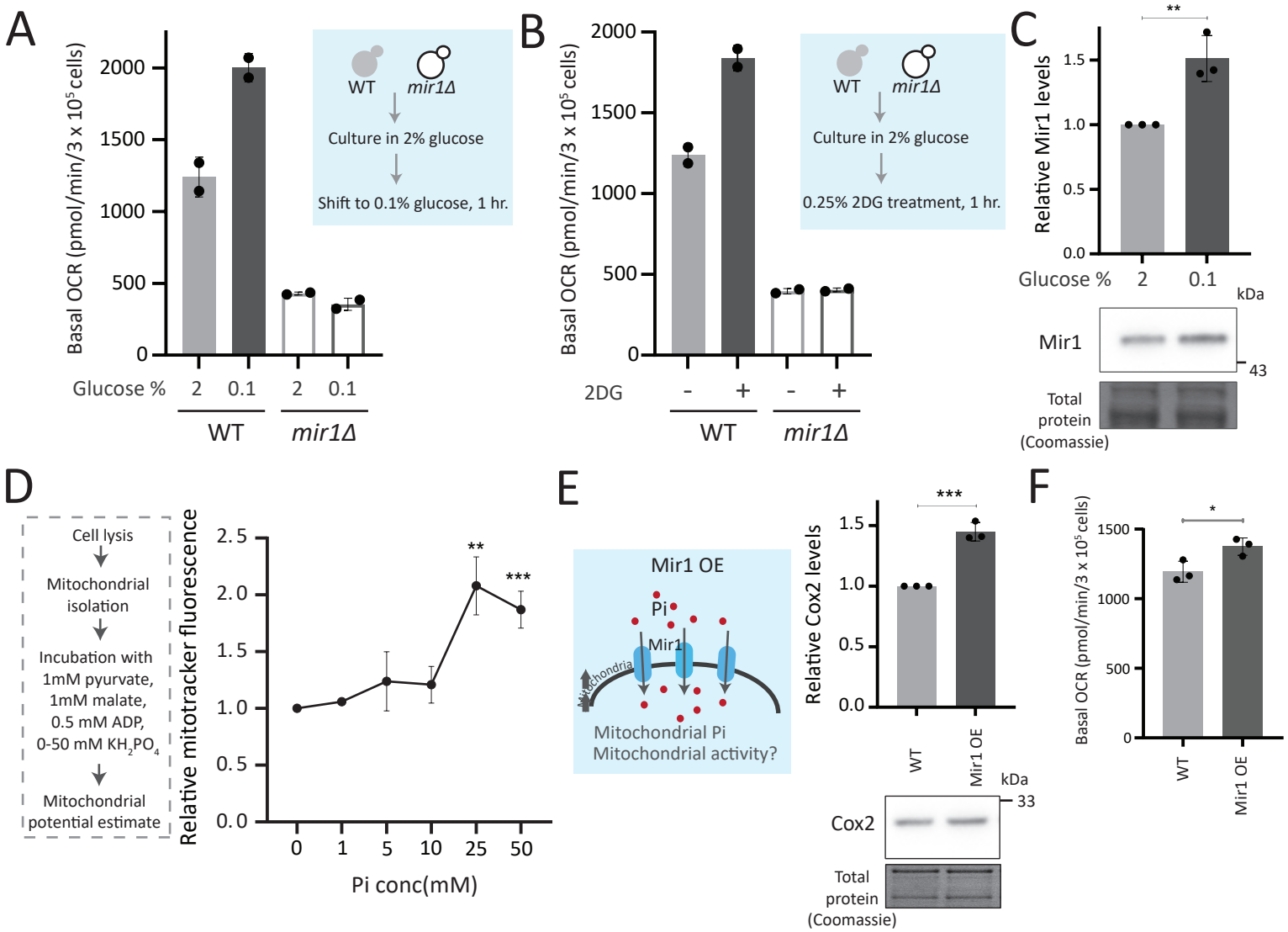

Figure 6: Ubp3 mediated regulation of mitochondrial respiration via Pi budgeting is conserved across different yeast strains

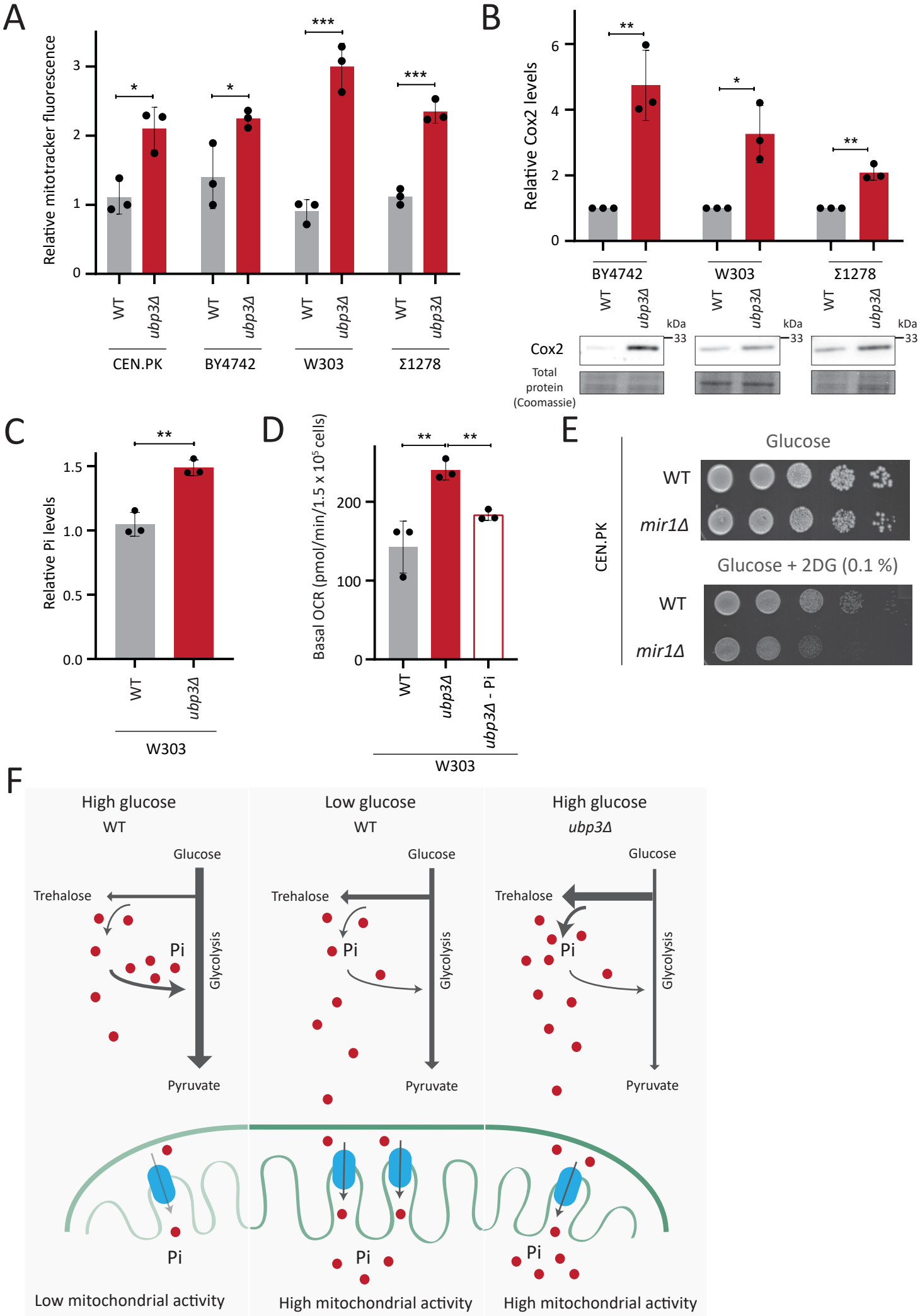

# Figure 1-figure supplement 1: DUB screen details and further characterization of Ubp3 functions

A

| Sl. No. | Gene name | Essential/ non-essential | Deleted in this study (Yes/No) | Mitotracker intensity of the deletion mutant (Relative to WT) | |
|---|---|---|---|---|---|
| 1 | Ubp1 | Non-essential | No. KOs were inviable | N/A | |
| 2 | Ubp2 | Non-essential | Yes | 0.832963 | 0.904247 |
| 3 | Ubp3 | Non-essential | Yes | 1.446586 | 1.632793 |
| 4 | Doa4 | Non-essential | Yes | 1.388516 | 1.221461 |
| 5 | Ubp5 | Non-essential | Yes | 1.073892 | 0.987076 |
| 6 | Ubp6 | Non-essential | Yes | 1.139659 | 1.040391 |
| 7 | Ubp7 | Non-essential | Yes | 0.961557 | 0.847109 |
| 8 | Ubp8 | Non-essential | Yes | 0.620714 | 0.98006 |
| 9 | Ubp9 | Non-essential | Yes | 0.923033 | 1.000494 |
| 10 | Ubp10 | Non-essential | Yes | 1.733428 | 1.636301 |
| 11 | Ubp11 | Non-essential | Yes | 1.03262 | 0.961782 |
| 12 | Ubp12 | Non-essential | Yes | 0.529191 | 0.602179 |
| 13 | Ubp13 | Non-essential | Yes | 0.972874 | 1.027698 |
| 14 | Ubp14 | Non-essential | Yes | 1.009835 | 0.864286 |
| 15 | Ubp15 | Non-essential | Yes | 0.898673 | 0.97787 |
| 16 | Ubp16 | Non-essential | Yes | 1.143826 | 0.993367 |
| 17 | Yuh1 | Non-essential | Yes | 0.9249 | 0.976146 |
| 18 | Otu1 | Non-essential | Yes | 0.944749 | 0.836696 |
| 19 | Otu2 | Non-essential | Yes | 0.854262 | 0.8604 |
| 20 | YGL082W | Non-essential | Yes | 1.39516 | 0.846423 |
| 21 | Rpn11 | Essential | No | N/A | |

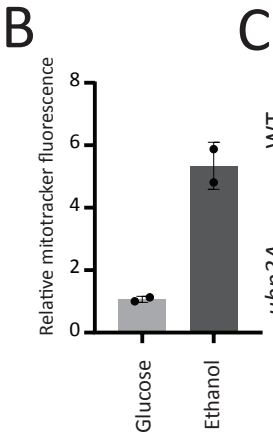


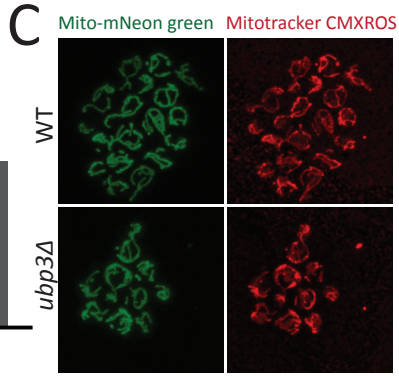


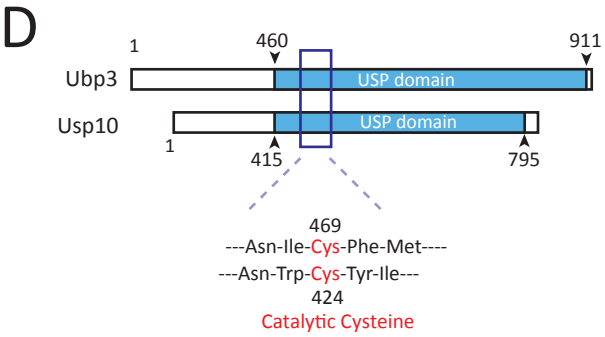


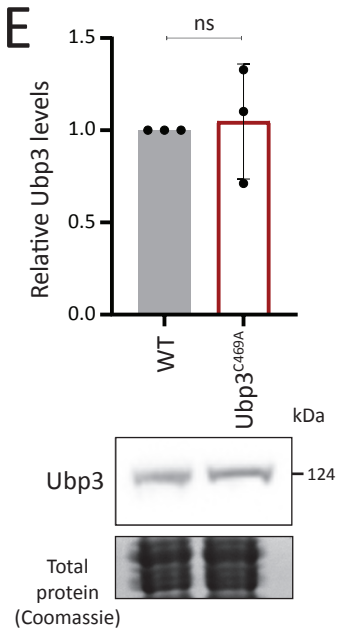


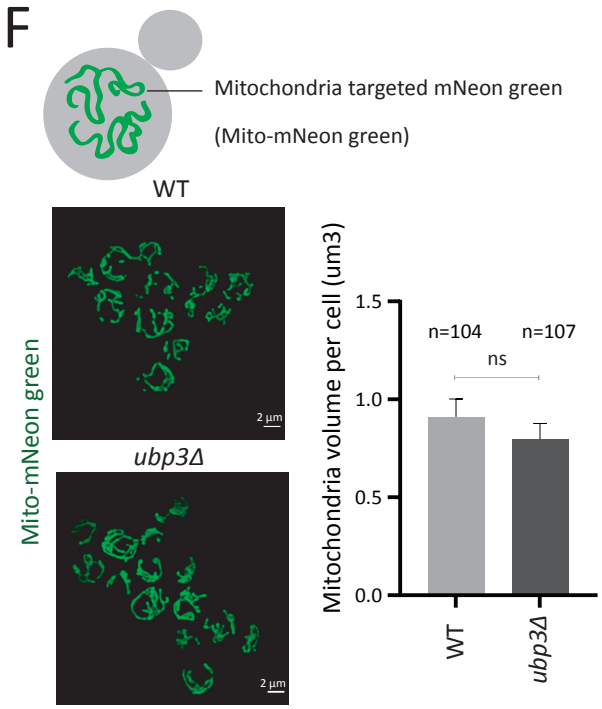


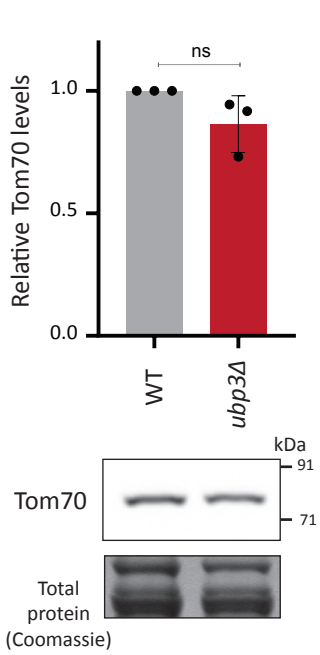


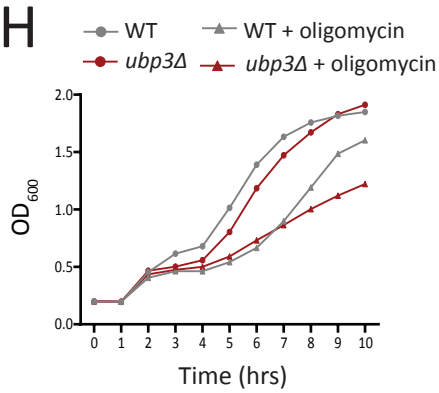


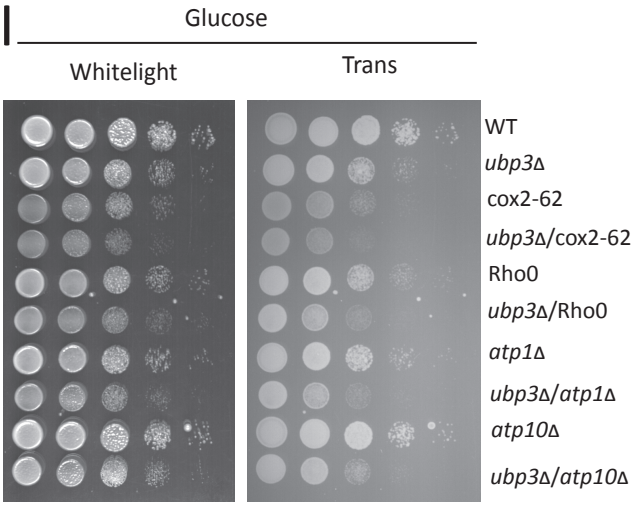


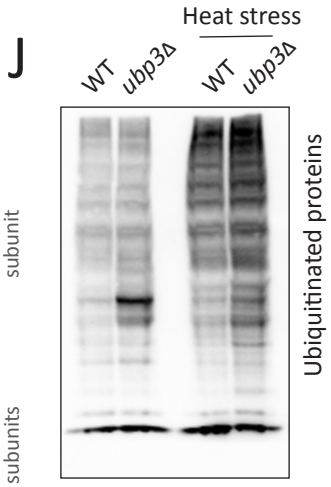

Figure 2-figure supplement 1: Further estimates of glycolytic enzymes and flux

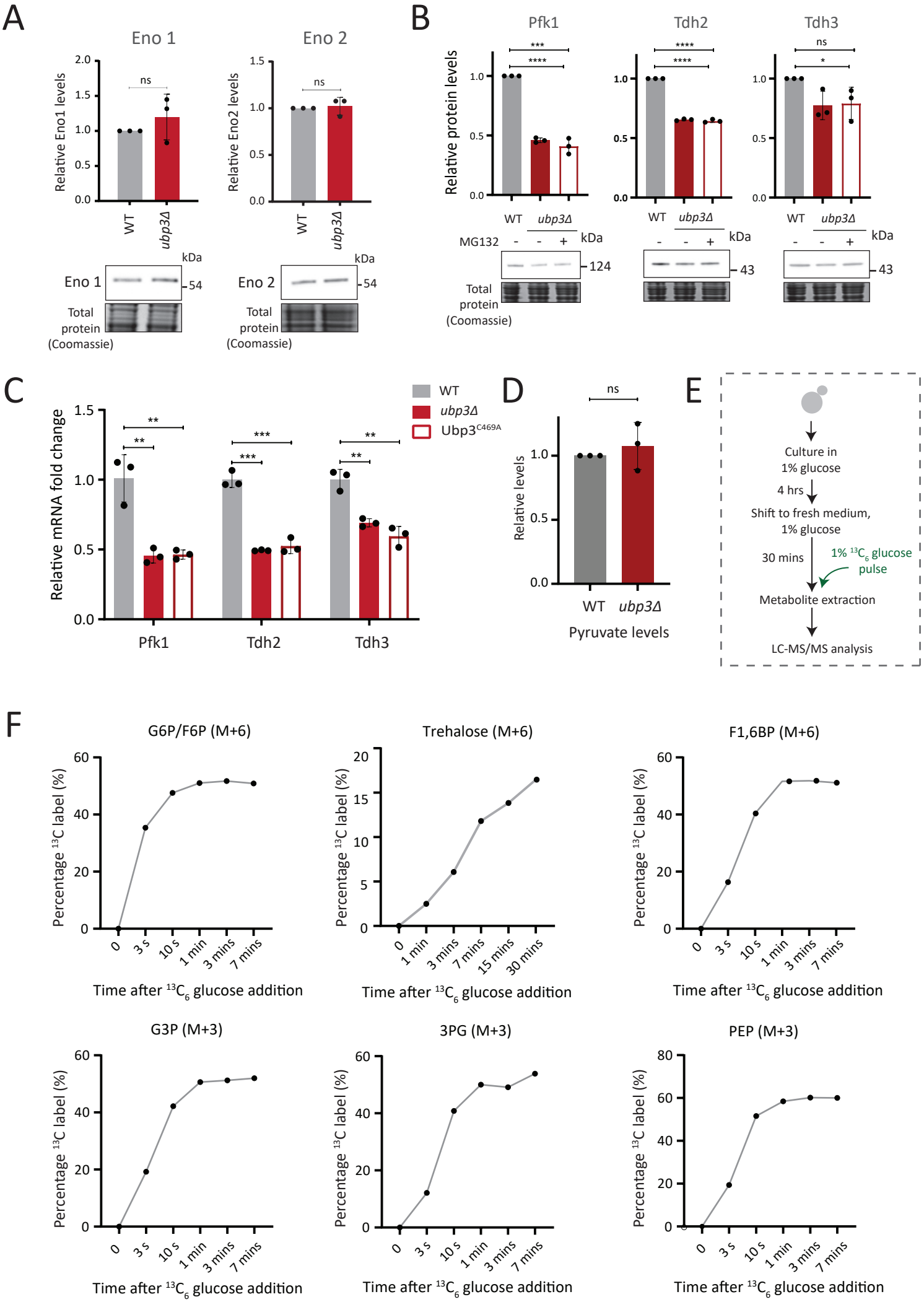

Figure 2-figure supplement 2: Estimation of steady state levels of metabolites and flux of TCA cycle intermediates

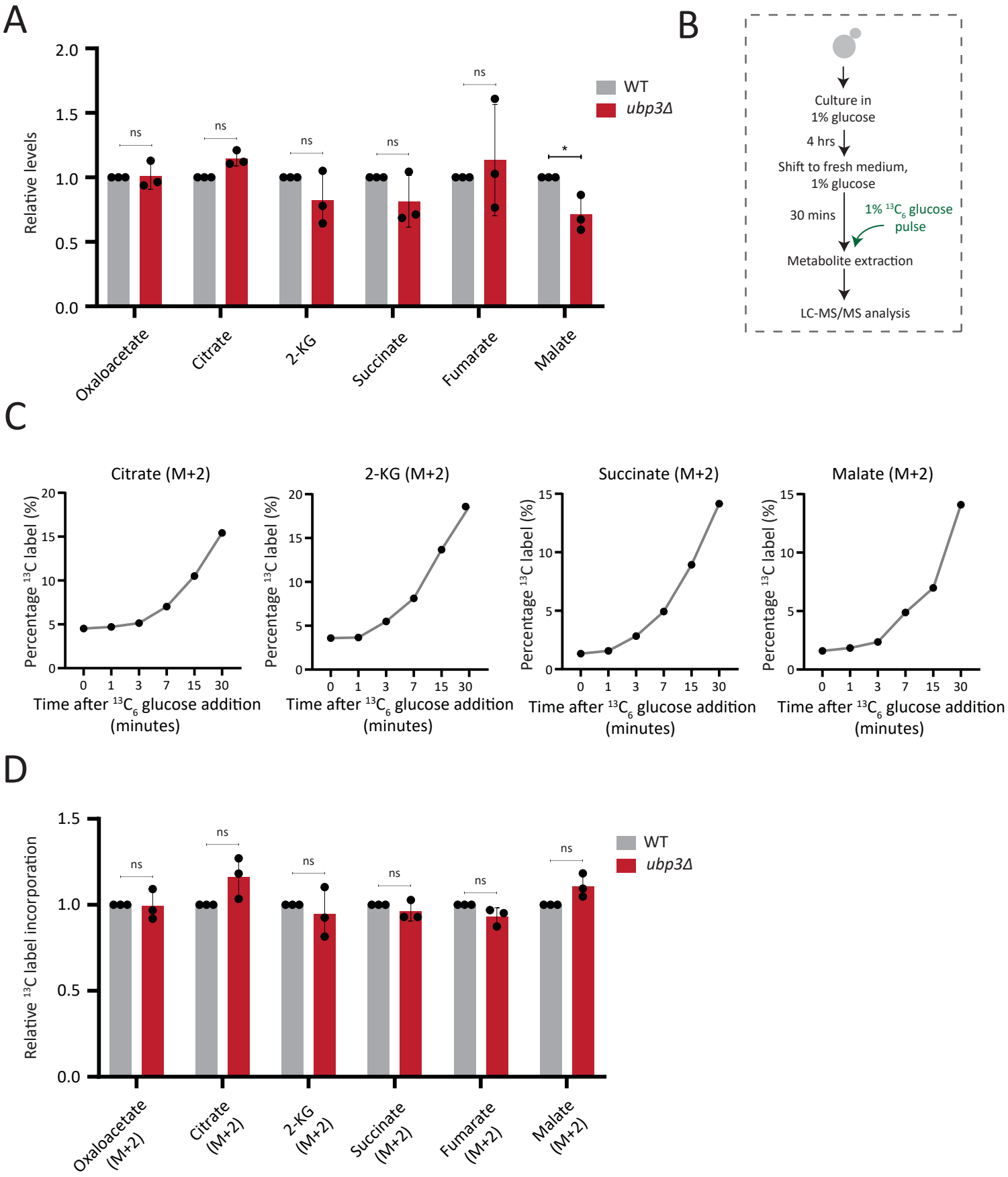

Figure 3-figure supplement 1: Comparisons of phosphate, ethanol and other metabolites in WT, *ubp3Δ* and GAPDH mutants

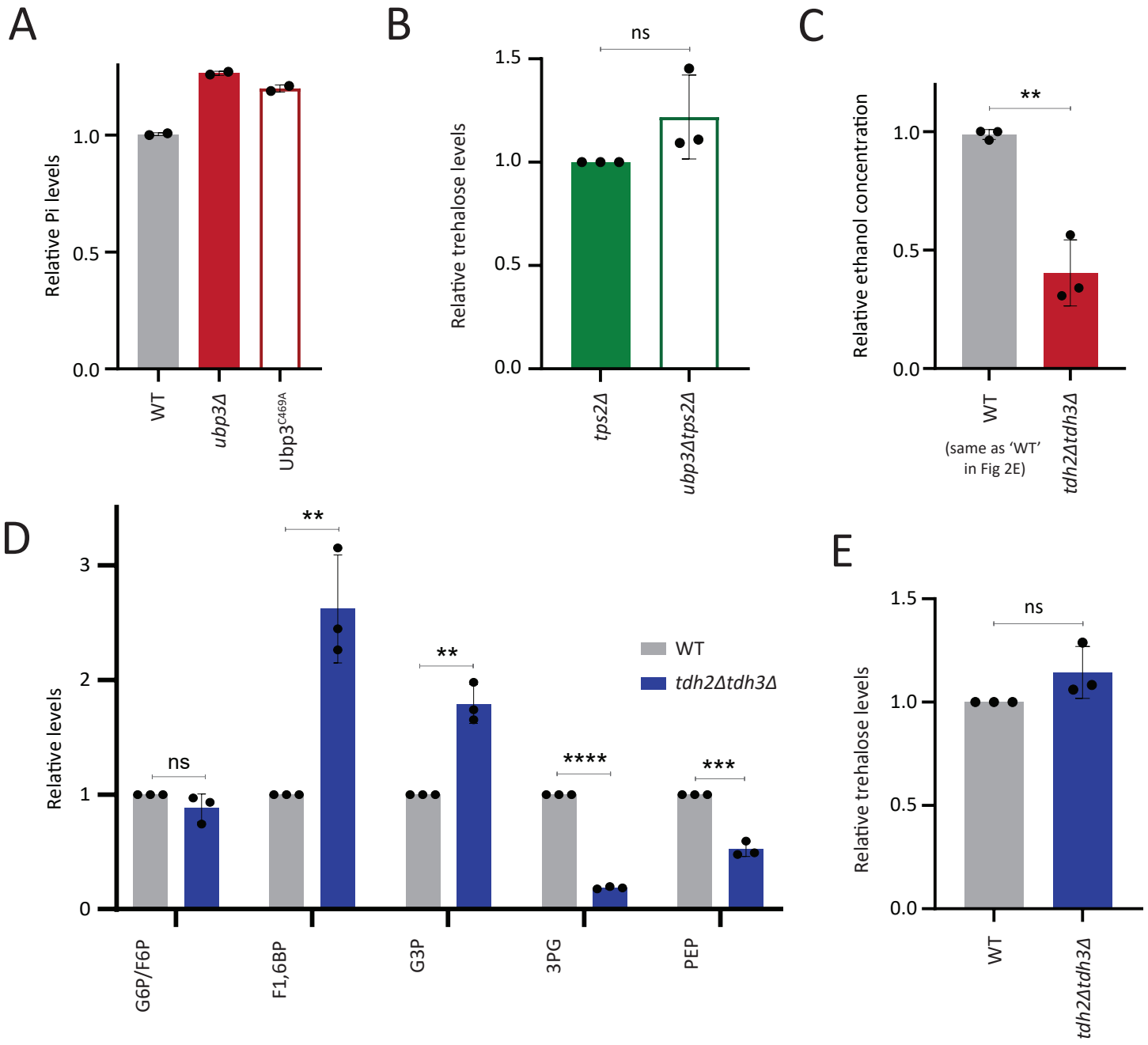

Figure 4-figure supplement 1: Mitochondrial Pi estimation characterizations and correlations of mitochondrial activity with Pi availability

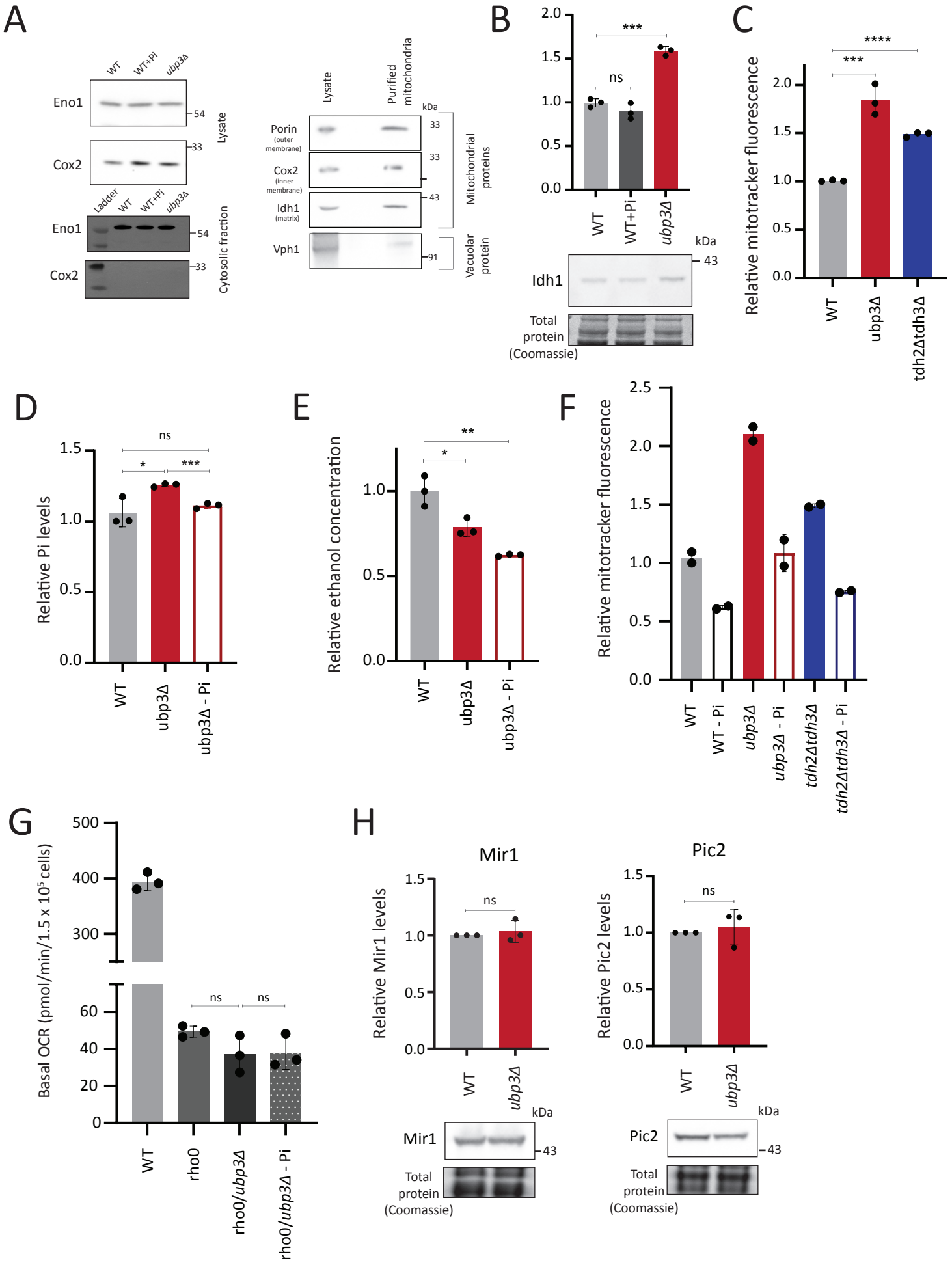
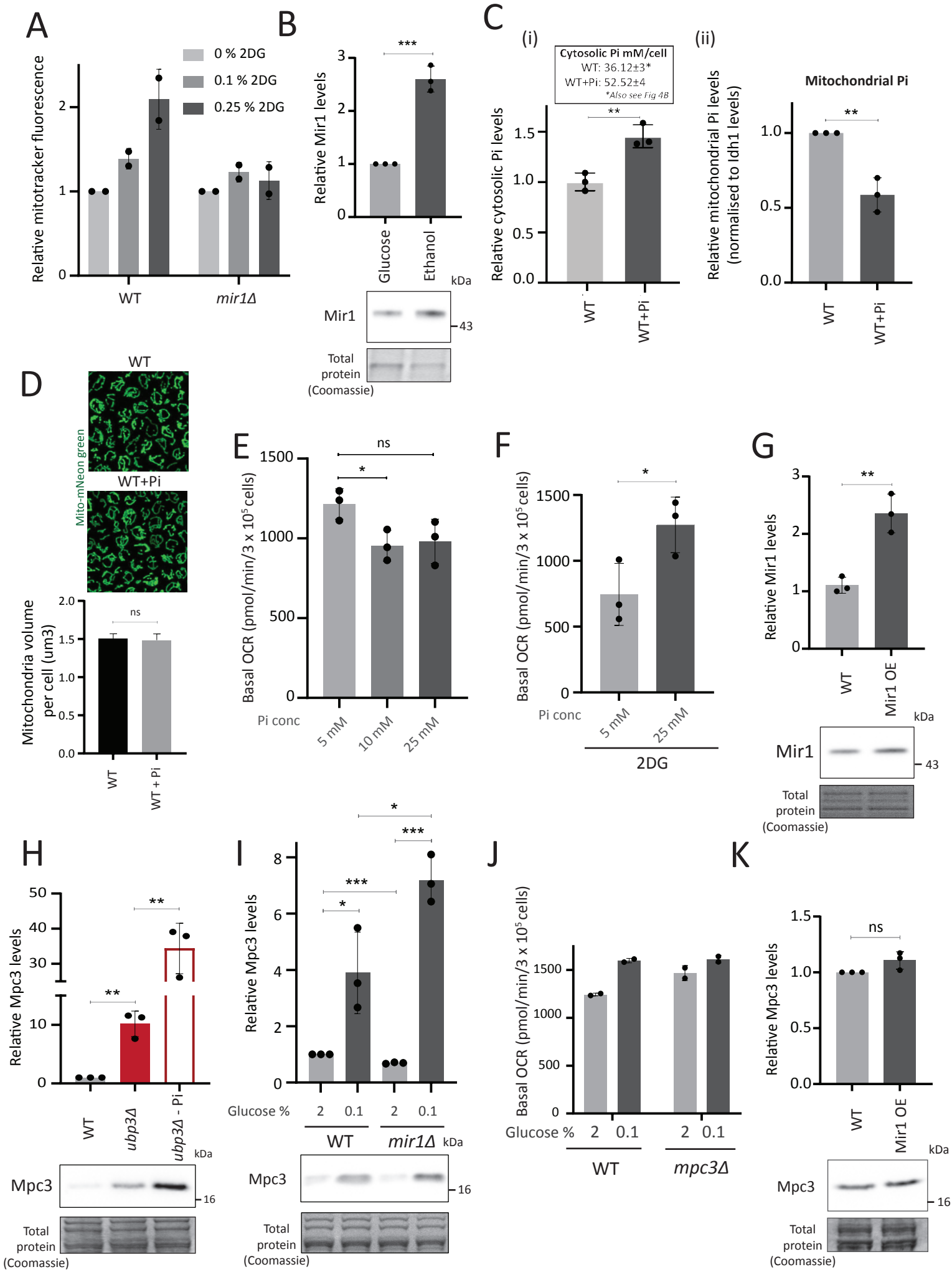
Figure 5-figure supplement 1: Mitochondrial phosphate and pyruvate transport relationships with mitochondrial activity